

# Regulation of the Volume-Regulated Anion Channel Pore-Forming Subunit LRRC8A in the Intrahippocampal Kainic Acid Model of Mesial Temporal Lobe Epilepsy

ASN Neuro  
Volume 15: 1–21  
© The Author(s) 2023  
Article reuse guidelines:  
sagepub.com/journals-permissions  
DOI: 10.1177/17590914231184072  
journals.sagepub.com/home/asn



Manolia R. Ghouli<sup>1,2</sup>, Carrie R. Jonak<sup>1,2</sup>, Rajan Sah<sup>3</sup>,  
Todd A. Fiacco<sup>2,4</sup> and Devin K. Binder<sup>1,2</sup> 

## Abstract

Volume-regulated anion channels (VRACs) are a group of ubiquitously expressed outwardly-rectifying anion channels that sense increases in cell volume and act to return cells to baseline volume through an efflux of anions and organic osmolytes, including glutamate. Because cell swelling, increased extracellular glutamate levels, and reduction of the brain extracellular space (ECS) all occur during seizure generation, we set out to determine whether VRACs are dysregulated throughout mesial temporal lobe epilepsy (MTLE), the most common form of adult epilepsy. To accomplish this, we employed the IHKA experimental model of MTLE, and probed for the expression of LRRC8A, the essential pore-forming VRAC subunit, at acute, early-, mid-, and late-epileptogenic time points (1-, 7-, 14-, and 30-days post-IHKA, respectively). Western blot analysis revealed the upregulation of total dorsal hippocampal LRRC8A 14-days post-IHKA in both the ipsilateral and contralateral hippocampus. Immunohistochemical analyses showed an increased LRRC8A signal 7-days post-IHKA in both the ipsilateral and contralateral hippocampus, along with layer-specific changes 1-, 7-, and 30-days post-IHKA bilaterally. LRRC8A upregulation 1 day post-IHKA was observed primarily in astrocytes; however, some upregulation was also observed in neurons. Glutamate-GABA/glutamine cycle enzymes glutamic acid decarboxylase, glutaminase, and glutamine synthetase were also dysregulated at the 7-day timepoint post status epilepticus. The time-point-dependent upregulation of total hippocampal LRRC8A and the possible subsequent increased efflux of glutamate in the epileptic hippocampus suggest that the dysregulation of astrocytic VRAC may play an important role in the development of epilepsy.

## Keywords

glutamate toxicity, glutamate-GABA/Glutamine cycle, hippocampal sclerosis, intrahippocampal kainic acid model, mesial temporal lobe epilepsy, volume-regulated anion channel

Received February 19, 2023; Revised May 22, 2023; Accepted for publication June 7, 2023

## Summary Statement

VRACs are upregulated primarily in astrocytes in the dorsal hippocampus at early and mid-epileptogenic periods, with variable layer-specific regulation following intrahippocampal kainate injection. The dysregulation of VRAC is paralleled by the dysregulation of GAD67, Glis1, and GS.

## Introduction

Mesial temporal lobe epilepsy (MTLE) is the most common form of adult epilepsy (Engel, 2001). MTLE is classified by seizures originating in mesial or limbic structures in the brain, such as the hippocampus, and is associated with a high risk of drug resistance (Engel et al., 2012). Available

<sup>1</sup>Division of Biomedical Sciences, School of Medicine, University of California—Riverside, Riverside, CA, USA

<sup>2</sup>Center for Glial-Neuronal Interactions, University of California—Riverside, Riverside, CA, USA

<sup>3</sup>Department of Internal Medicine, Washington University School of Medicine, St. Louis, MO, USA

<sup>4</sup>Department of Cell Biology and Neuroscience, University of California—Riverside, Riverside, CA, USA

## Corresponding Author:

Devin K. Binder, 2120 Multidisciplinary Research Building, University of California, Riverside, Riverside, CA 92521-0121, USA.

Email: dbinder@ucr.edu



anti-seizure drugs (ASDs) work to decrease neuronal hyper-synchronization by targeting neuronal channels and receptors. However, one-third of epilepsy patients become refractory to these therapies (Kwan and Brodie, 2000). Therefore, it is imperative that novel, non-neuronal therapeutic targets are developed as part of future-generation ASDs.

The glutamate–gamma-aminobutyric acid (GABA)/glutamine cycle has gained significant attention in the epilepsy field. The fact that glutamate is responsible for seizures and excitotoxic damage is rooted in the finding that seizures can be caused by disruptions to the glutamate–GABA/glutamine cycle that favors excitatory glutamatergic neurotransmission. Perturbations to the glutamate–GABA/glutamine cycle that increase the concentration of extracellular glutamate cause tonic activation of glutamate receptors and subsequently drives  $\text{Ca}^{2+}$  into neurons, triggering neuronal necrosis and apoptosis (Bukke et al., 2020). Because of their indispensable role in the glutamate–GABA/glutamine cycle, astrocytes are a key component of the glutamate toxicity hypothesis and may serve as novel, non-neuronal ASD targets. Astrocytes clear glutamate from the extracellular space and either metabolize it through the tricarboxylic acid cycle or convert it into its neutral equivalent, glutamine, which is recycled back to neurons. Previous studies have shown that astroglial glutamate transporters and the glutamate-to-glutamine converting enzyme glutamine synthetase (GS) are critical for the maintenance of the ambient extracellular glutamate concentration, and their dysregulation leads to seizures (Rothstein et al., 1996; Tanaka et al., 1997). However, because glutamate transport into astrocytes is concentrative, astrocytes are a potential source of glutamate back into the ECS if glutamate-permeable channels on the cell membrane become available.

Volume-regulated anion channels (VRACs) are outward rectifiers that are permeable to glutamate and offer a nonvesicular mechanism for astroglial glutamate release (Yang et al., 2019; Zhou et al., 2020). VRACs are hexameric channels composed of LRRC8 subunits (LRRC8A–E), with evidence that LRRC8A is required to form functional pores (Hydzinski-García et al., 2014; Qiu et al., 2014; Serra et al., 2021; Voss et al., 2014). In the presence of adenosine triphosphate (ATP), VRACs are activated by cell swelling, and mediate regulatory volume decrease (RVD) through an efflux of anions and organic osmolytes, thereby creating an osmotic gradient to drive water out of the cell to ultimately restore the cell volume. Interestingly, the ablation of LRRC8A from nestin<sup>+</sup> cells results in premature adolescent death due to seizure activity (Wilson et al., 2021). Nestin is an intermediate filament expressed in neuronal precursor cells that later differentiate into neurons, astrocytes, and oligodendrocytes, so this suggests that LRRC8A—and, by extension, VRACs—are necessary for normal nervous system development and for maintaining neuronal homeostasis (Bernal and Arranz, 2018). In astrocytes, LRRC8A was determined to be essential for the generation of swelling-induced chloride currents and for the mediation of RVD (Formaggio et al., 2019). Furthermore, the conditional deletion of LRRC8A from glial fibrillary acidic protein (GFAP<sup>+</sup>) astrocytes attenuated neuronal excitability and protected

against ischemic brain damage in an experimental model of stroke (Yang et al., 2019). Although the mechanism through which LRRC8A contributes to ischemia-induced brain injury has yet to be determined, the leading hypothesis in the field suggests VRAC-mediated glutamatergic input to hippocampal neurons may mediate excitotoxic damage (Zhou et al., 2020). These studies suggest that the conditional deletion of LRRC8A from specific cell types such as astrocytes may prevent the assembly of functional VRAC pores, thereby attenuating VRAC-mediated astroglial glutamate efflux and preventing excitotoxicity.

We hypothesize that astroglial VRAC-mediated glutamate efflux may contribute to neuronal hyperexcitability and the development of an epileptic phenotype. We set out to determine: (a) whether hippocampal VRAC are dysregulated during development of MTL; (b) whether the dysregulation of VRAC occurs in astrocytes and/or neurons and varies across different time points during the development of MTL; and (c) whether there are changes in the levels of other glutamate–GABA/glutamine cycle machinery at the time points of maximal VRAC dysregulation. An aberrant expression of VRAC may play a causal role in the development of epilepsy, suggesting this channel may serve as a candidate therapeutic target in the development of future-generation ASDs.

## Materials and Methods

### Animals

Eight- to ten-week-old wild-type male C57BL/6J mice (Jackson Labs) were used in this study. In Western blot experiments, 4–5-week-old SWELL<sup>fl/fl</sup>; Nestin<sup>CRE/+</sup> mice were also used as a negative control to validate VRAC expression. SWELL<sup>fl/fl</sup>; Nestin<sup>CRE/+</sup> mice were not age-matched with the C56BL/6J mice because they expired prematurely between 5 and 6 weeks of age as described previously (Wilson et al., 2021; Yang et al., 2019; Zhou et al., 2020). To generate SWELL<sup>fl/fl</sup>; Nestin<sup>CRE/+</sup> mice, SWELL<sup>fl/fl</sup> mice generated by Dr. Rajan Sah (Washington University) were crossed with Nestin<sup>CRE</sup> mice (Jackson Labs, strain 003771). The mice were housed under a 12-h light/dark cycle and provided standard rodent chow and water *ad libitum*. All procedures were conducted with approval from the University of California Institutional Animal Care and Use Committee (IACUC) and in accordance with the NIH Animal Care and Use Guidelines. A total of 83 mice were used in this study.

### Intrahippocampal Kainic Acid Model

Animals were anesthetized in an isoflurane chamber (0.2%–0.5%, Covetrus) and then given an i.p. injection of 80 mg/kg ketamine (Zoetis, 10004027) and 10 mg/kg xylazine (Bimeda, 1XYL003). Toe pinches were conducted to determine the level of anesthesia throughout the surgical procedure, and supplemental doses of ketamine/xylazine were

administered as needed. Once anesthetized, the head was shaved, aseptically prepared for surgery, and securely placed in a stereotaxic apparatus. A midsagittal incision was made, and the skull was exposed with a cotton-tipped applicator. A burr hole was placed 1.8 mm posterior and 1.6 mm lateral to bregma. Animals received a 46 nL intrahippocampal kainic acid (IHKA) injection (20 mM kainic acid, Tocris Bioscience 0222) via a microinjector (Nanoject III, Drummond Sci.) into the CA1 region (1.9 mm ventral) of the hippocampus as previously described (Hubbard et al., 2016; Lee et al., 2012). Control animals received a 46 nL intrahippocampal sterile saline injection (0.9%, Covetrus). Following the surgery, animals were sutured, treated with triple antibiotic ointment, given a subcutaneous injection of 0.1 mg/kg buprenorphine (Reckitt & Colman, 5053624), and placed on a heating pad to aid in recovery. Animals were video recorded for 5 h following surgery to confirm the development of status epilepticus (SE). The International League Against Epilepsy (ILAE) defines SE as “a condition resulting either from the failure of the mechanisms responsible for seizure termination or from the initiation of mechanisms, which lead to abnormally, prolonged seizures” (Trinka et al., 2015, p. 1515). This ultimately results in an enduring epileptic condition constituting neuronal injury, neuronal death, and neuronal network alteration (Beghi, 2020). In our model, SE is defined by the presence of at least 3 Racine level 4–5 seizure events within 5 h following IHKA (Racine, 1972). Fifty-seven animals underwent IHKA; however, four of these animals did not meet the Racine qualifications to be included in the study. Animals that developed SE were collected at various timepoints corresponding to critical periods in epileptogenesis. These included 1-day post-IHKA (1dKA), coinciding with acute SE-mediated changes; 7-days post-IHKA (7dKA), coinciding with early epileptogenic changes and the onset of spontaneous seizures in this model; 14-days post-IHKA (14dKA), coinciding with mid-epileptogenic changes; and 30-days post-IHKA (30dKA), coinciding with chronic epileptogenic changes (Lee et al., 2012; Peterson and Binder, 2019; Peterson et al., 2021) (Figure 1).

### Immunohistochemistry

Animals were euthanized in an isoflurane chamber, perfused first with ice-cold phosphate-buffered saline (1× PBS), then with ice-cold 4% paraformaldehyde (PFA) 1-, 7-, 14-, and 30-days post-IHKA and post-sham surgeries. The animal brains were harvested, fixed in 4% PFA for two hours at room temperature, transferred to 30% sucrose and stored at 4°C until the brains sank. The brains were flash frozen for 1 min in isopentane, and then stored at –80°C until use. Frozen brains were sealed in optimum cutting temperature (O.C.T.) formulation and sliced into 50 µm sections at 20°C using a cryostat (Leica CM 1950). The sections were stored in 1× PBS with 0.01% sodium azide. For each animal, three sections of the hippocampus proximal to the injection site were collected and processed via immunohistochemistry (IHC). The sections were washed with PBS, incubated in

3% hydrogen peroxide to quench endogenous peroxidase activity, washed with PBS, blocked in 10% BSA/ 5% Triton X-100 (in PBS), and incubated in primary antibodies (Abcam ab157489 anti-LRRC8A, EMD Millipore MAB360 anti-mGFAP, Proteintech 12855-1-AP anti-KGA/GAC, EMD Millipore G2781 anti-GS, EMD Millipore MAB5406 anti-GAD67, and EMD Millipore MAB377 anti-NeuN) overnight at 4°C. The following day, sections were washed with PBS, incubated in Alexa Fluor secondary antibodies with the aid of a Tyramide Amplification Kit, and mounted onto glass slides with ProLong™ Gold Antifade Mountant with DAPI. Slides were imaged using a Leica microscope and processed with Leica software (LAS-X). The images were quantified using Fiji Image J software. The images were converted to 8-bit files, and regions of interest (ROIs) were established in the DAPI channel. The total hippocampus, as well as the following layers of the hippocampus, was analyzed: *stratum oriens* (SO), *stratum pyramidale CA1* (CA1), *stratum radiatum* (SR), *stratum lacunosum moleculare* (SLM), molecular layer (ML), *upper granule cell layer* (GCL<sub>U</sub>), *hilus* (H), *lower granule cell layer* (GCL<sub>L</sub>), *stratum pyramidale CA3* (CA3), and *stratum lucidum* (SL) (Figure 2). The mean gray values were measured for LRRC8A signal blinded to time points and treatment. Colocalization of LRRC8A with GFAP or NeuN signals was determined with a Fiji Image J colocalization plugin (author: Pierre Bourdoncle, Institut Jacques Monod, Service Imagerie, Paris). This plugin highlights the colocalized points of two 8-bit images and the colocalized points will appear white, after which the program combines the three 8-bit images into an RGB image. Two points are only considered to be colocalized if their respective intensities are strictly higher than the threshold of their channels (which are 50 by default: Threshold channel 1 (0–255)), and if their ratio (of intensity) is strictly higher than the ratio setting value (which is 50% by default: ratio (0%–100%)). Representative confocal images were taken using an Olympus BX61 confocal microscope (Olympus America Inc., Center Valley, PA, USA), and z-stack projections were performed using CellSens.

### Western Blot Analysis

A separate cohort of animals from all the established timepoints was euthanized in an isoflurane chamber and perfused with ice-cold PBS/protease inhibitor cocktail. Dorsal hippocampal and cortical tissues were separately harvested via microdissection, placed in safe-lock tubes with an ice-cold RIPA buffer/protease inhibitor cocktail, homogenized, and centrifuged. The supernatant was extracted and aliquoted into Eppendorf tubes and stored at –80°C until use. The protein concentration of samples was quantified against a Bradford assay and measured with a BioTek Synergy 2 plate reader. 10% sodium dodecyl sulfate (SDS)-polyacrylamide gels (1.5 mm, 10-well, 66 µL/well) were made immediately prior to use. Homogenized samples were denatured with 4× Laemmli buffer, 20% SDS, and water at 55°C for 10 min, and then kept on ice. Gels were submerged in a running buffer, samples were loaded into the gels, and the gels were run at 50 V for 30 min

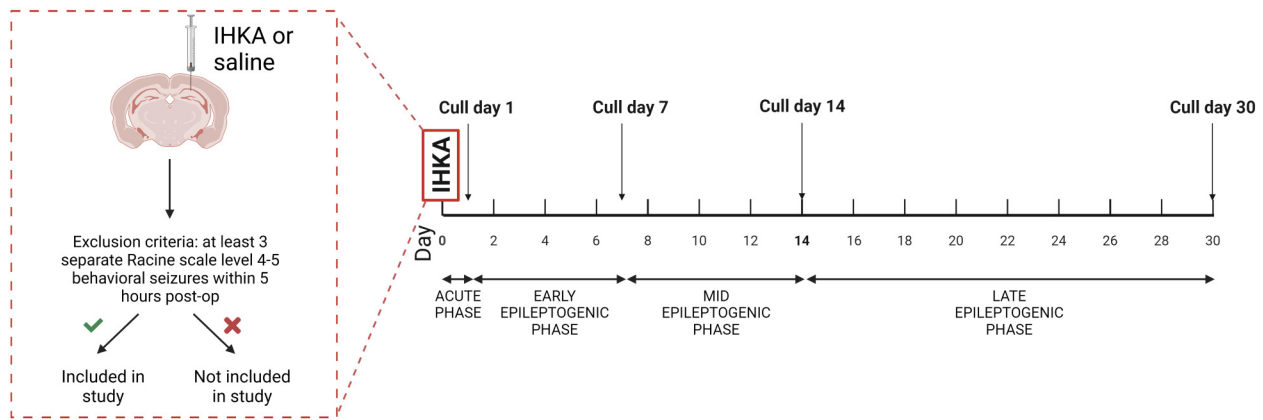


**Figure 1.** Overview of the experimental timeline.

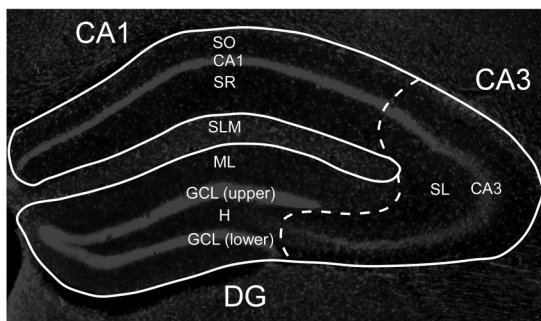


**Figure 2.** Overview of the hippocampal layers.

and then run at 125 V for 2 h on ice. Gels were transferred to nitrocellulose membranes at 30 V overnight (18.5 h) at 4°C. Membranes were washed, blocked in TBS with 5% milk for 1 h at room temperature, and then incubated in primary antibodies (1:100 Cell Signaling Technology LRRC8A/ SWELL1 Antibody #24979, 1:1000 Sigma anti- $\beta$ -actin A1978) overnight in 4°C. Membranes were washed, incubated in LI-COR IRDye secondary antibodies (1:250 goat anti-rabbit IR 680, and 1:10,000 mouse anti-mouse IR 800), washed again, and imaged with LI-COR Odyssey Fc and analyzed with Image Studio (version 5.2). The ROIs were established with the same area for each lane/band. The LRRC8A signal was normalized against the  $\beta$ -actin signal of the same lane. Importantly, attempts to generate an LRRC8A protein band using the Abcam primary Anti-LRRC8A antibody (ab157489) failed, despite this antibody providing LRRC8A signal in IHC when paired with a tyramide signal amplification kit. However, the Cell Signaling Technology primary LRRC8A/SWELL1 Antibody (#24979) reliably produced robust bands on WB.

### Quantification and Statistical Analysis

Raw numerical data were processed with Microsoft Excel (Microsoft Corp., Seattle, WA, USA), and all statistical analyses were conducted with Prism 9 software (GraphPad Software, La

Jolla, CA, USA). Datasets were evaluated for normality and equal variance. Datasets that met these assumptions were then analyzed *via* a two-tailed *t*-test or—in the case of multiple comparisons—*via* one-way ANOVA with *post hoc* Dunnett's multiple comparisons tests. Datasets that did not meet these assumptions were analyzed *via* non-parametric Mann-Whitney-*U* test or—in the case of multiple comparisons—*via* Kruskal-Wallis nonparametric tests with *post hoc* Dunn's multiple comparisons tests. Brown-Forsythe revealed saline controls from 7-, 14-, and 30-day timepoints exhibited no significant differences ( $P > .05$ , Brown-Forsythe), therefore saline-treated controls were grouped together. All data points were depicted in figures. All error bars represent the mean  $\pm$  standard error of the mean (SEM). Statistical significance was denoted as follows: \* indicates  $P$ -value  $< .05$ , \*\* indicates  $P$ -value  $< .01$ , \*\*\* indicates  $P$ -value  $< .001$ , and \*\*\*\* indicates  $P$ -value  $< .0001$ .

## Results

### Validation of the IHKA Model in the Development of MTLE

The most common histopathological finding in resected murine and human brains with MTLE is hippocampal sclerosis (HS) (Baulac, 2015). HS develops due to the prolonged seizure exposure and is marked by thinning of CA1 pyramidal layer neurons, granule cell dispersion, and reactive gliosis. To validate the development of HS in this model, both GFAP immunoreactivity and GCL width were measured in the ipsilateral and contralateral hippocampi at 1dKA, 7dKA, 14dKA, and 30dKA and compared to grouped saline-injected controls ( $n = 5-7$  KA-treated animals,  $n = 15$  control animals).

In the ipsilateral hippocampus, total GFAP immunoreactivity was found to be increased at 14dKA ( $F(4,32) = 3.072$ ,  $P = .0300$ , one-way ANOVA;  $P = .0251$ , 95% C.I. =  $[-19.26, -1.005]$ , *post hoc* Dunnett's test). Layer-specific quantification revealed increased GFAP immunoreactivity at 7dKA in SO, CA1, SR, SLM, and CA3; at 14dKA in SO, CA1, SR, SLM, H, and CA3; and at 30dKA in SO,



CA1, SR, SLM, and CA3 (all  $p < .05$  by *post hoc* Dunn's test or Dunnett's test) (Figures 3A and B). The GCL width in the ipsilateral hippocampus was found to be increased at 7dKA and 14dKA ( $H(4) = 22.33$ ,  $P = .0002$ , Kruskal–Wallis; 7dKA  $P = .0102$  and 14dKA  $P = .0003$  by *post hoc* Dunn's test). High-magnification images of GFAP<sup>+</sup> astrocytes revealed significant hypertrophy of

these cells in KA-treated tissue compared to saline-treated tissue in the ipsilateral hippocampus (Figure 3C). The increase in GFAP immunoreactivity and astroglial hypertrophy are indicative of astrogliosis, and the increase in GCL width points to granule cell dispersion. These findings confirm the development of HS in the ipsilateral hippocampus of KA-treated animals.

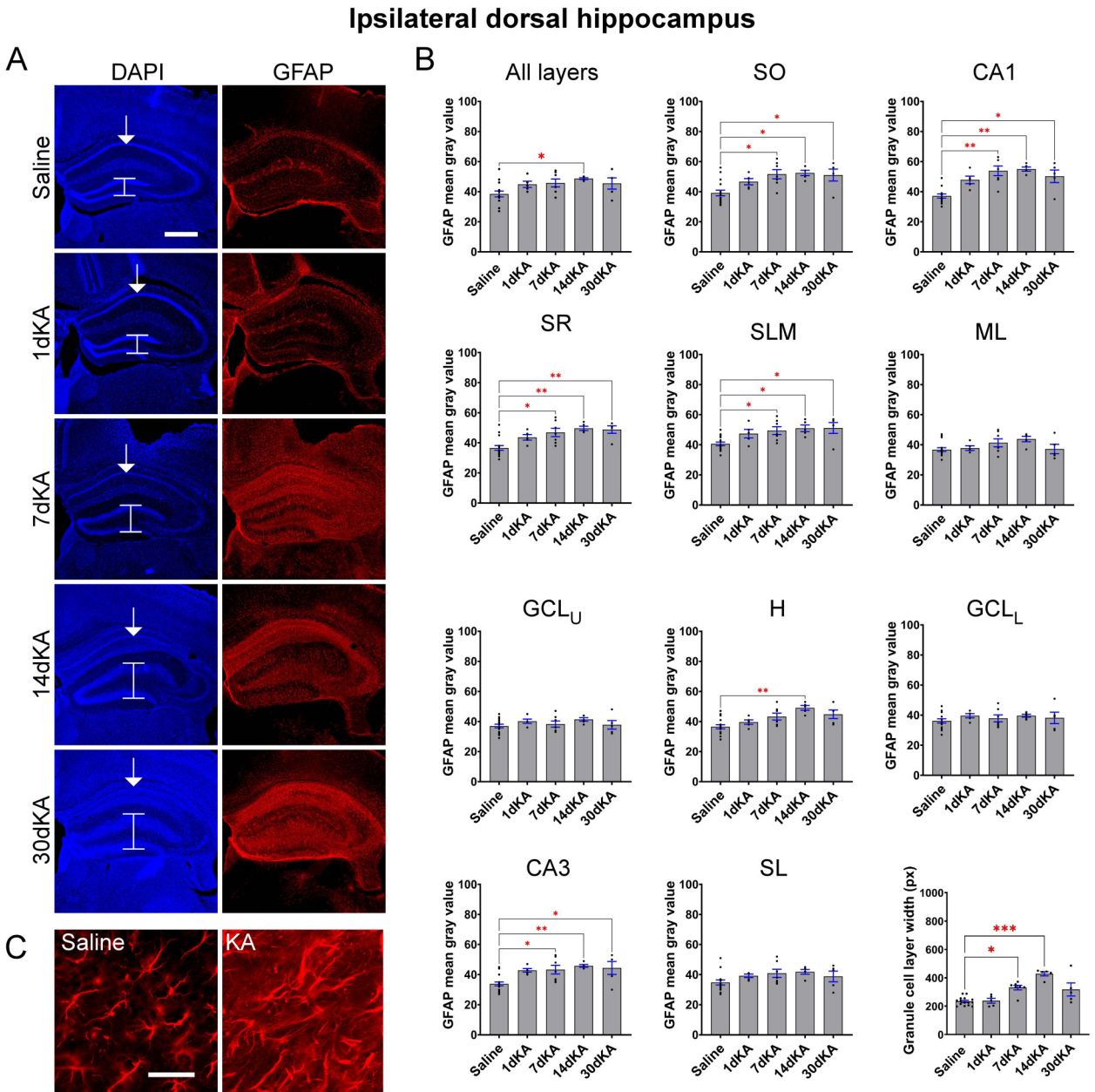


**Figure 3.** Validation of the IHKA model in the development of MTLE in the ipsilateral hippocampus. (3A) Representative images of the ipsilateral dorsal hippocampus from the saline control tissue as well as 1-day post-IHKA (1dKA), 7-days post-IHKA (7dKA), 14-days post-IHKA (14dKA), and 30-days post-IHKA (30dKA) demonstrating the progressive development of three key characteristics of HS in the IHKA model of epilepsy: (1) thinning of the CA1 pyramidal cell layer (white arrows, visualized via DAPI immunofluorescence), (2) granule cell dispersion (white lines, visualized via DAPI immunofluorescence), and (3) gliosis as observed via GFAP immunofluorescence. (3B) Total hippocampus (all layers) and layer-specific mean gray value quantification of GFAP immunofluorescence, as well as the measured width of the GCL in the ipsilateral hippocampus. \* indicates  $P < .05$ , \*\* indicates  $P < .01$ , and \*\*\* indicates  $P < .001$ . Scale bar: 500  $\mu\text{m}$ . (3C) High-resolution images of astrocyte morphology comparing saline-treated and KA-treated tissues (30dKA) from the ipsilateral hippocampus. Scale bar: 50  $\mu\text{m}$ .



( $F(4, 33) = 1.037$ ,  $P = .4029$ , one-way ANOVA). As observed in the ipsilateral hippocampus, high-magnification images of GFAP<sup>+</sup> astrocytes reveal significant hypertrophy of these cells in KA-treated tissues compared to saline-treated tissues in the contralateral hippocampus (Figure 4C). Although the contralateral hippocampus exhibited astrogliosis, it did not show evidence of granule cell dispersion, pointing to a partial HS phenotype.

### Total Dorsal Hippocampal LRRC8A is Upregulated at 14dKA as Detected via Immunoblot

To validate the immunoblot detection of LRRC8A using the anti-LRRC8A antibody, the hippocampal and cortical LRRC8A content of wild-type (WT) C57BL6 and SWELL1<sup>fl/fl</sup>; Nestin<sup>CRE/+</sup> animals were assessed (Figure 2A). SWELL1<sup>fl/fl</sup>; Nestin<sup>CRE/+</sup>

animals served as a negative control, as these animals exhibit the conditional deletion of LRRC8A—also termed SWELL1—in nestin<sup>+</sup> neural progenitors. Nestin expression is multicellular during neurogenesis, making it an optimal promoter to execute a widespread deletion of LRRC8A in the adult central nervous system (Bernal and Arranz, 2018). The expression of LRRC8A normalized against  $\beta$ -actin was reduced both in the hippocampus ( $t(df) = 11.27(2)$ ,  $P = .0078$ , mean  $\pm$  SEM:  $-4.600 \pm 0.4081$ , two-tailed  $t$ -test) and in the cortex ( $t(df) = 7.660(2)$ ,  $P = .0166$ , mean  $\pm$  SEM:  $-7.351 \pm 0.9597$ , two-tailed  $t$ -test) of the cKO tissue compared to the WT tissue (Figures 5A and B).

Next, changes in the LRRC8A expression throughout epileptogenesis were evaluated *via* immunoblot ( $n = 5-8$  animals per KA-treated group,  $n = 20$  control animals). In both the ipsilateral (Figure 5C) and contralateral (Figure 5E) hippocampus, a main

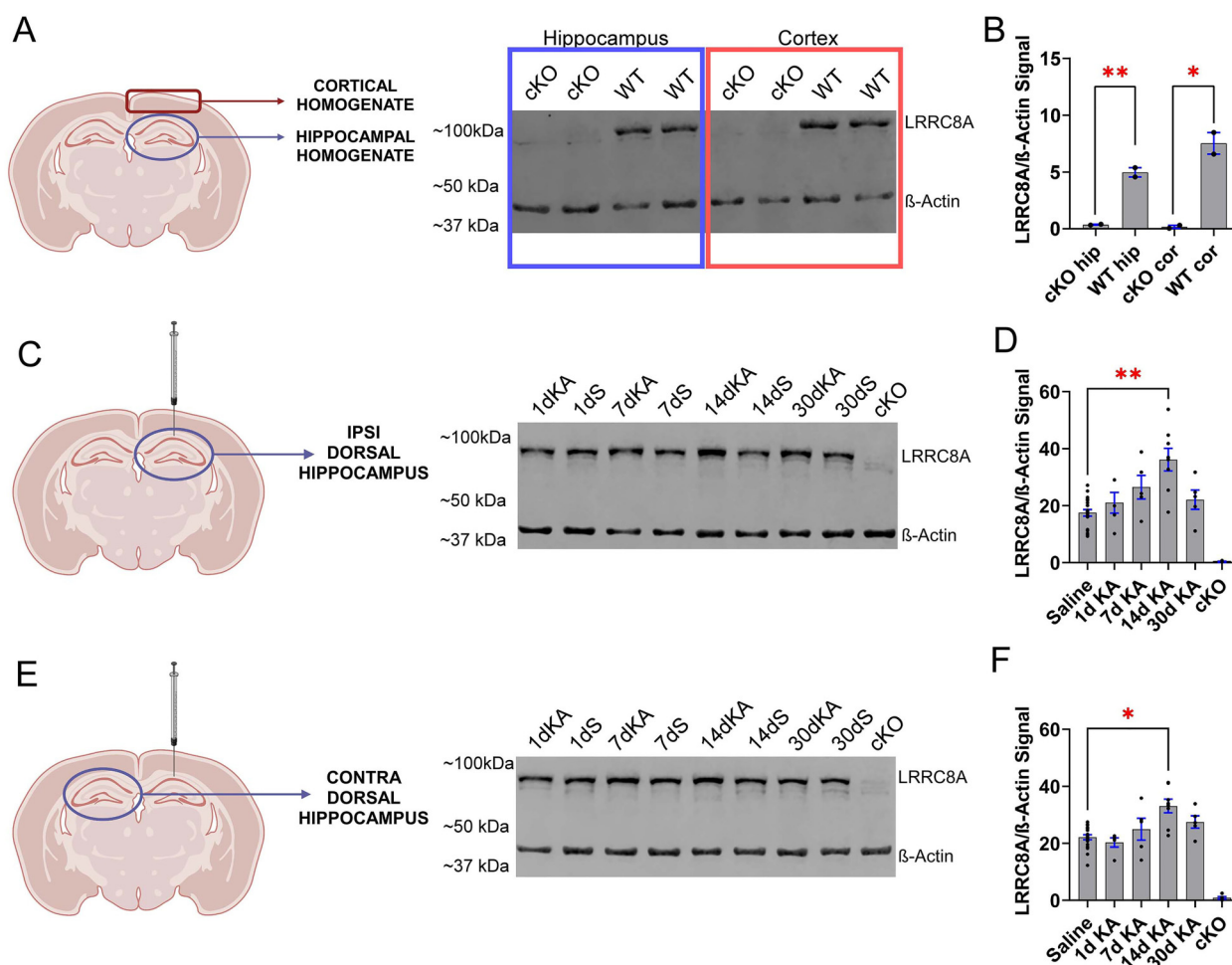


**Figure 5.** Total dorsal hippocampal LRRC8A is upregulated at 14dKA as detected via immunoblot. (5A) Representative blot of LRRC8A and  $\beta$ -actin immunodetection from the hippocampal and cortical tissues of both WT and SWELL1<sup>fl/fl</sup>; Nestin<sup>CRE/+</sup> (cKO) animals ( $n = 2$ ), and (5B) the respective quantification of the LRRC8A expression normalized against  $\beta$ -actin. Sample blots of ipsilateral (5C) and contralateral (5E) dorsal hippocampus samples at 1dKA, 7dKA, 14dKA, and 30dKA with respective saline-injected control samples and an additional cKO control lane. Quantification of the ipsilateral (5D) and contralateral (5F) LRRC8A expressions normalized against  $\beta$ -actin from KA-treated animals compared to grouped saline-treated controls.  $n = 5$  was used for all time points except for 14dKA for which  $n = 8$  was used. \* indicates  $P < .05$  and \*\* indicates  $P < .01$ . Partly created with BioRender.com.



effect of timepoint on the LRRC8A expression was observed ( $H(5) = 26.42$ ,  $P < .0001$  ipsilateral;  $H(5) = 25.94$ ,  $P < .0001$  contralateral, Kruskal–Wallis). Specifically, the LRRC8A expression was significantly elevated at 14dKA in both hemispheres compared to saline controls ( $P = .0023$  ipsilateral (Figure 5D);  $P = .0110$  contralateral (Figure 5F), *post hoc* Dunn's test). These data suggest that the LRRC8A expression is upregulated in both the ipsilateral and contralateral dorsal hippocampus at 14dKA, the mid-epileptogenic period.

### Total Dorsal Hippocampal LRRC8A is Upregulated at 7dKA with Variable Layer-Specific Regulation Throughout Epileptogenesis as Detected via IHC

Next, changes in the LRRC8A expression throughout epileptogenesis were evaluated *via* IHC ( $n = 3–5$  animals per KA-treated group,  $n = 13$  control animals). In the total ipsilateral hippocampus (Figure 6A), LRRC8A immunoreactivity was increased at 7dKA ( $H(4) = 22.05$ ,  $P = .0002$ , Kruskal–Wallis;

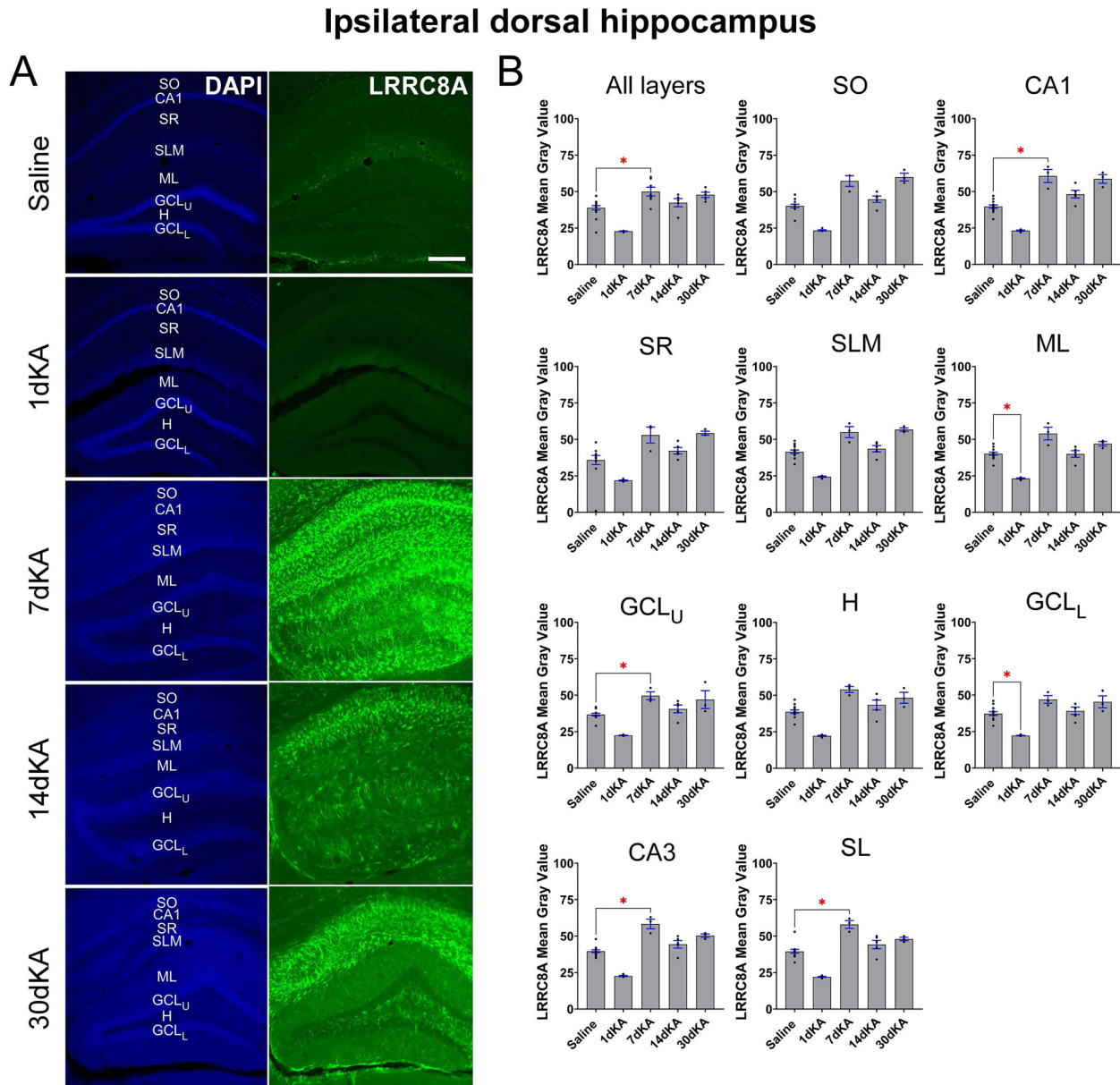


**Figure 6.** LRRC8A immunoreactivity in the ipsilateral dorsal hippocampus after IHKA. (6A) Representative 10× magnification immunofluorescence images of the ipsilateral dorsal hippocampus from saline-treated control tissues and KA-treated tissue at 1dKA, 7dKA, 14dKA, and 30dKA stained for DAPI (blue) and LRRC8A (green). Specific layers of the hippocampus are outlined in DAPI (SO, CA1, SR, SLM, ML, GCL<sub>U</sub>, H, GCL<sub>L</sub>, CA3, and SL). (6B) Total hippocampus (all layers) and layer-specific mean gray value quantification of LRRC8A immunofluorescence in the ipsilateral dorsal hippocampus at 1dKA, 7dKA, 14dKA, and 30dKA compared to grouped saline control (min.  $n = 3$  and max.  $n = 8$  animals per group, 2–3 sections per animal). \* indicates  $P < .05$ . Scale bar: 250  $\mu\text{m}$ .

$P = .0253$ , *post hoc* Dunn's test), with layer-specific increases or decreases depending on the time points. Layer-specific decreases were observed at 1dKA in ML and GCL<sub>L</sub> (both  $P < .05$  by *post hoc* Dunn's test). In contrast, layer-specific increases were observed at 7dKA, including CA1, GCL<sub>U</sub>, CA3, and SL (all  $P < .05$  by *post hoc* Dunn's test) (Figure 6B).

In the contralateral hippocampus (Figure 7A), LRRC8A immunoreactivity was similarly increased at 7dKA ( $H(4) = 22.74$ ,  $P = .0001$ , Kruskal–Wallis;  $P = .0220$ , *post hoc* Dunn's

test) with layer-specific increases or decreases depending on the time points. Layer-specific decreases were observed at 1dKA in GCL<sub>U</sub>, H, and GCL<sub>L</sub> (all  $P < .05$  by *post hoc* Dunn's test). Alternately, layer-specific increases were observed at 7dKA in SO, CA1, SR, CA3, and SL; and at 30dKA in SO, CA1, SR, and SLM (all  $P < .05$  by *post hoc* Dunn's test) (Figure 7B).

Overall, the immunohistochemical data highlight the upregulation of total hippocampal LRRC8A signal in both the ipsilateral and

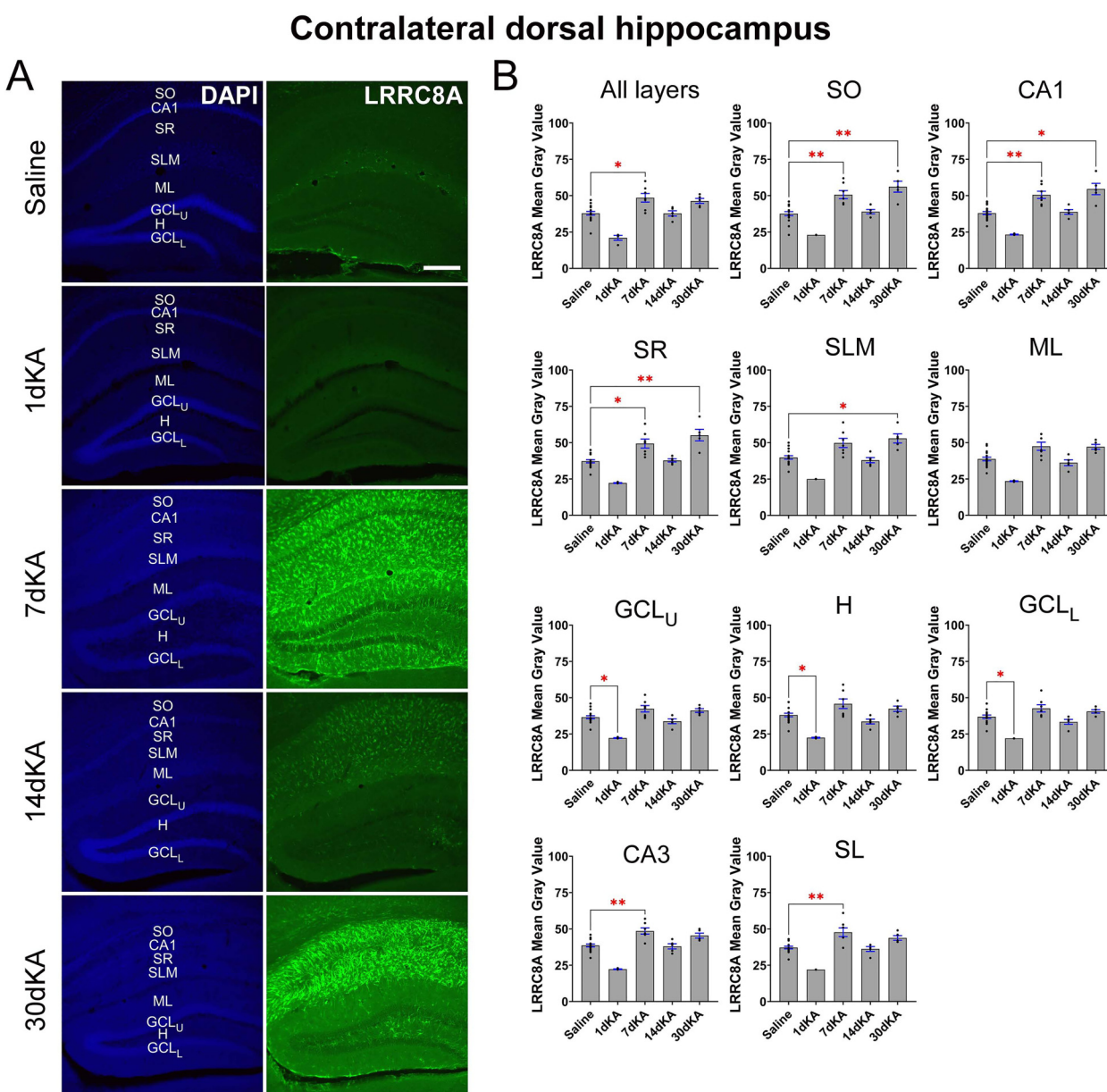


**Figure 7.** LRRC8A immunoreactivity in the contralateral dorsal hippocampus after IHKA. (7A) Representative 10× magnification immunofluorescence images of the contralateral dorsal hippocampus from saline-treated control tissue and KA-treated tissue at 1dKA, 7dKA, 14dKA, and 30dKA stained for DAPI (blue) and LRRC8A (green). Specific layers of the hippocampus are outlined in DAPI (SO, CA1, SR, SLM, ML, GCL<sub>U</sub>, H, GCL<sub>L</sub>, CA3, and SL). (7B) Total hippocampus (all layers) and layer-specific mean gray value quantification of LRRC8A immunofluorescence in the contralateral dorsal hippocampus at 1dKA, 7dKA, 14dKA, and 30dKA compared to grouped saline control (min.  $n = 3$  and max.  $n = 8$  animals per group, 2–3 sections per animal). \* indicates  $P < .05$  and \*\* indicates  $P < .01$ . Scale bar: 250  $\mu\text{m}$ .

contralateral dorsal hippocampus at 7dKA, the early epileptogenic period. Layer-specific analysis revealed more nuanced changes in LRRC8A, with decreased signal at 1dKA in specific layers of both the ipsilateral (ML and GCL<sub>L</sub>) and contralateral (GCL<sub>U</sub>, H, and GCL<sub>L</sub>) dorsal hippocampus; increased signal at 7dKA both ipsilaterally (CA1, GCL<sub>U</sub>, CA3, and SL) and contralaterally (SO, CA1, SR, CA3, and SL); and an increased signal at 30dKA in the contralateral hippocampus (SO, CA1, SR, and SLM).

### ***Increased LRRC8A Immunoreactivity Colocalizes with GFAP at 7dKA***

It is important to determine whether the increased LRRC8A immunoreactivity at 7dKA was occurring in neurons or astrocytes. First, the colocalized immunoreactivity of LRRC8A with GFAP, an astrocytic marker, was evaluated in the dorsal hippocampus of KA-treated and control animals at 7dKA ( $n=6$  KA-treated animals,  $n=4$  saline controls, 1–2 sections per condition).

LRRC8A and GFAP were found to be colocalized in the ipsilateral hippocampus (saline median colocalization: 13), and KA treatment significantly increased colocalization by a factor of 3.85 (KA median colocalization: 50; KA vs. saline: Mann–Whitney  $U=3$ ,  $P<.0001$  two-tailed  $t$ -test) (Figures 8A and B). Similar observations were made in the contralateral hippocampus where KA treatment significantly increased LRRC8A and GFAP colocalization by a factor of 5.71 (KA vs. saline: Mann–Whitney  $U=20$ ,  $P=.0111$  two-tailed  $t$ -test) (Figures 8D and E).

As described above, at 7dKA, the LRRC8A signal intensity was significantly greater in the ipsilateral hippocampal layers CA1, GCL<sub>U</sub>, CA3, and SL; and in the contralateral hippocampal layers SO, CA1, SR, CA3, and SL. High-resolution 40× representative images of LRRC8A and GFAP colocalization in these layers suggest that LRRC8A is considerably upregulated in GFAP<sup>+</sup> astrocytes in the ipsilateral (Figure 8C) and contralateral (Figure 8F) KA-treated hippocampus. However, there is an occasional LRRC8A labeling in GFAP<sup>-</sup> cells—likely non-astrocytic cells (white arrows).

### ***LRRC8A is Partially Upregulated in NeuN<sup>+</sup> Neurons at 7dKA***

To determine whether LRRC8A was upregulated in neurons, the colocalized immunoreactivity of LRRC8A with NeuN, a neuronal marker, was evaluated in the dorsal hippocampus of KA-treated and control mice at 7dKA ( $n=6$  KA-treated animals,  $n=4$  saline controls, 1–2 sections per condition). LRRC8A and NeuN were found to be colocalized only following IHKA (saline median colocalization: 0, KA median colocalization: 11;  $P<.01$  KA vs. saline) (Figures 9A and B). In the contralateral hippocampus, LRRC8A was not found to be colocalized with NeuN in either condition

(saline median colocalization: 0.00, KA median colocalization: 0.00) (Figures 9D and E).

High-resolution 40× representative images of LRRC8A and NeuN colocalization in the specific hippocampal layers of maximal LRRC8A signal intensity at 7dKA also showed no clear colocalization of LRRC8A with NeuN<sup>+</sup> signal either in the ipsilateral (Figure 9C) or contralateral (Figure 9F) dorsal hippocampus. Colocalization of LRRC8A with NeuN was sparse in stratum pyramidale and the GCL (white arrows) in control tissues, with no measurable difference after kainate treatment, suggesting that LRRC8A is not significantly upregulated in neurons in epileptic tissues.

To summarize, at 7dKA, LRRC8A staining was significantly more intense bilaterally in GFAP<sup>+</sup> cells, with little change in the sparse LRRC8A and NeuN colocalization in KA-treated versus control tissues. These data suggest that LRRC8A colocalizes mainly with astrocytes and that an increased expression and the immunolabeling of LRRC8A are predominantly astrocytic at the early epileptogenic time point in this MTL model.

### ***Changes to Glutamate/GABA–Glutamine Cycle at 7dKA***

Having determined that LRRC8A is dysregulated predominantly in astrocytes in the hippocampus at 7dKA, it was intriguing to discern whether any other glutamate-handling machinery was altered at this timepoint. Previously, it was determined that there is a robust downregulation of GLT-1 and EAAC1 at 7dKA (Peterson and Binder, 2019; Peterson et al., 2021), suggesting aberrant glutamate re-uptake in the epileptic hippocampus. In an effort to assess the glutamate/GABA–glutamine cycle more comprehensively in the present study, the immunoreactivity of glutamic acid decarboxylase isoform 67 (GAD67), glutaminase (Gls1), and glutamate synthetase (GS) were evaluated at 7dKA in both the ipsilateral and contralateral dorsal hippocampus.

In the ipsilateral hippocampus, total GAD67 immunoreactivity was significantly decreased in KA-treated animals compared to controls (Mann–Whitney  $U=7$ ,  $P=.0063$  two-tailed  $t$ -test) (Figure 10A), with layer-specific decreases observed in CA1, SLM, ML, GCL<sub>U</sub>, GCL<sub>L</sub>, CA3, and SL (all  $P<.05$  by Mann–Whitney–Wilcoxon test) (Figure 10B). Similarly, in the contralateral hippocampus, total GAD67 immunoreactivity was significantly decreased in KA-treated animals compared to controls (Mann–Whitney  $U=9.5$ ,  $P=.0039$  two-tailed  $t$ -test), with layer-specific decreases observed in SR, ML, and GCL<sub>U</sub> (all  $P<.05$  by Mann–Whitney–Wilcoxon test) (Figure 10C).

As for Gls1, in the ipsilateral hippocampus, total Gls1 immunoreactivity was significantly decreased in KA-treated animals compared to controls (Mann–Whitney  $U=4.5$ ,  $P=.0023$  two-tailed  $t$ -test) (Figure 11A), with significant layer-specific decreases observed in SO, SR, SLM, H, and



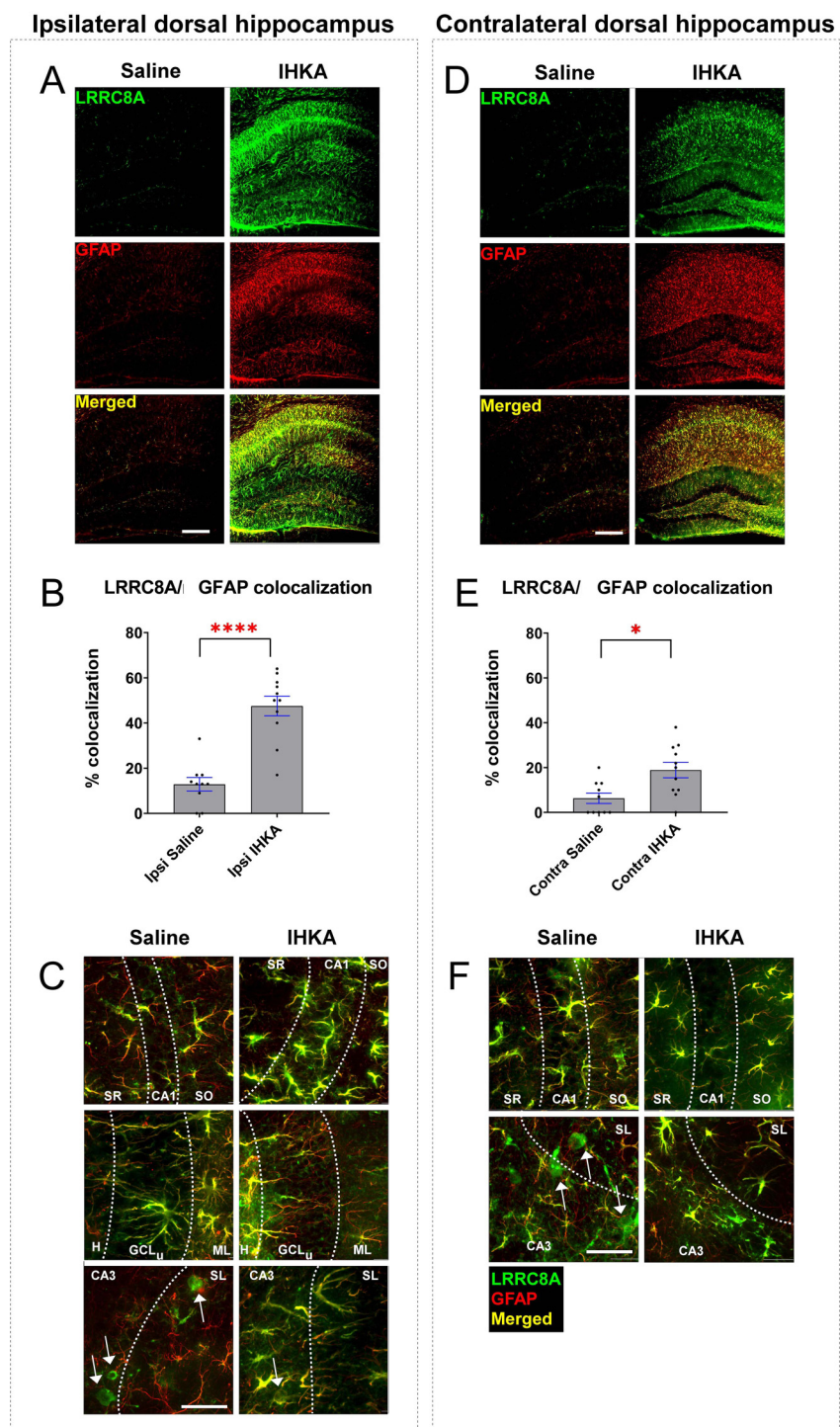


**Figure 8.** Increased LRRC8A immunoreactivity colocalizes with GFAP at 7dKA. Representative images of the ipsilateral (8A) and contralateral (8D) dorsal hippocampus from saline-treated control and KA-treated tissue stained for LRRC8A (green) and GFAP (red). LRRC8A/GFAP colocalization is visualized in the merged images (yellow). Scale bar: 250  $\mu$ m. Quantification of LRRC8A/GFAP colocalization in the ipsilateral (8B) and contralateral (8E) dorsal hippocampus. \* indicates  $P < .05$  and \*\*\*\* indicates  $P < .0001$ . High-magnification representative images of colocalization in saline-treated control and KA-treated tissues in the hippocampal layers that were determined to exhibit LRRC8A upregulation at 7dKA in the ipsilateral hippocampus (CA1, GCL<sub>U</sub>, SL, and CA3; 8C) and contralateral hippocampus (SO, CA1, SR, SL, and CA3; 8F). White arrows point to the LRRC8A signal that does not colocalize with the GFAP signal (likely neuronal cell bodies). Scale bar: 50  $\mu$ m.

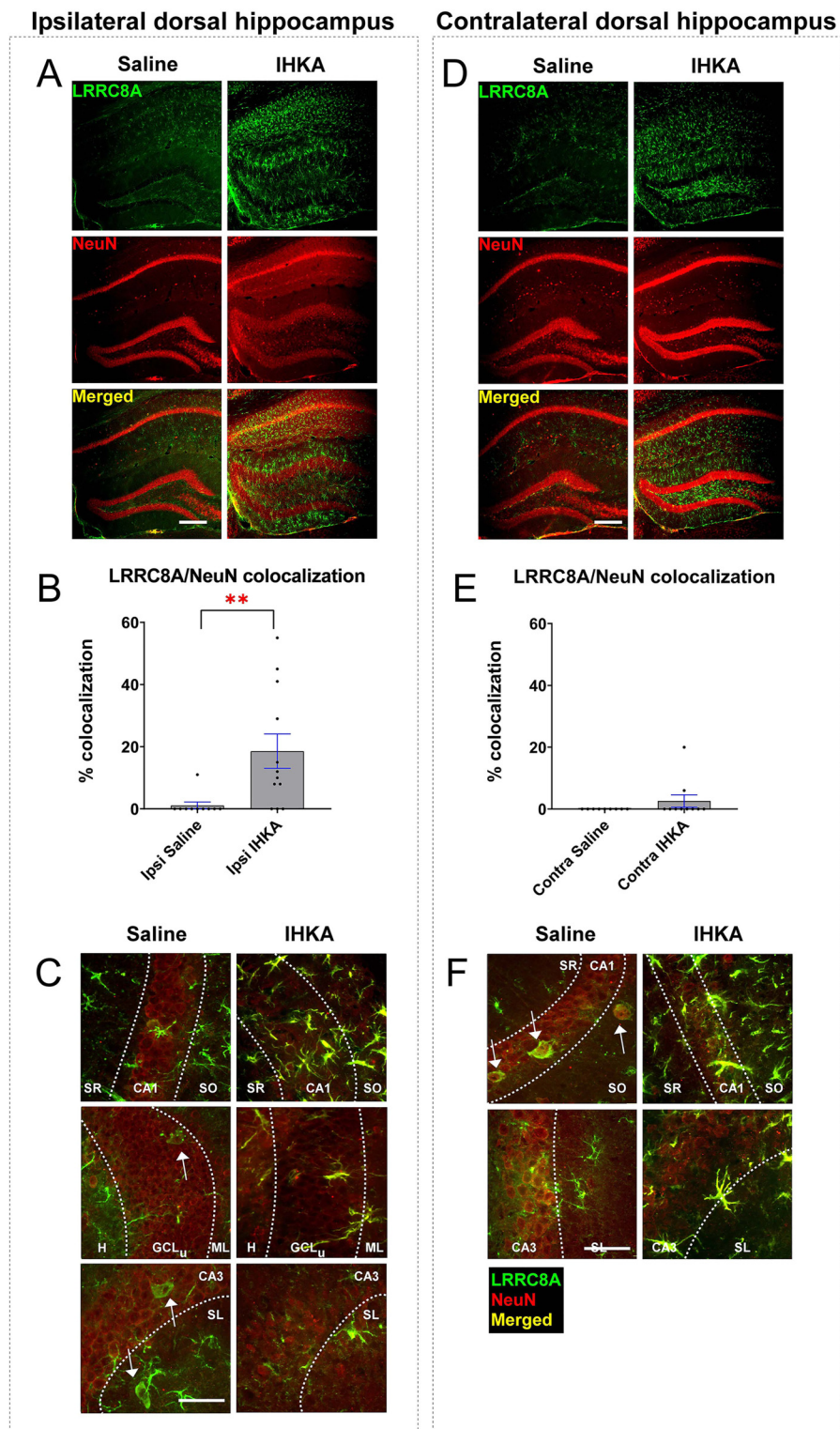


**Figure 9.** LRRC8A is partially upregulated in NeuN<sup>+</sup> neurons at 7dKA. Representative images of the ipsilateral (9A) and contralateral (9D) dorsal hippocampus from saline-treated control and KA-treated tissue stained for LRRC8A (green) and NeuN (red). LRRC8A/NeuN colocalization is visualized in the merged images (yellow). Scale bar: 250  $\mu$ m. Quantification of LRRC8A/NeuN colocalization in the ipsilateral (9B) and contralateral (9E) dorsal hippocampus. \*\* indicates  $P < .01$ . High-magnification representative images of colocalization in saline-treated control and KA-treated tissues in the hippocampal layers that exhibit LRRC8A upregulation at 7dKA in the ipsilateral hippocampus (CA1, GCL<sub>u</sub>, SL, and CA3; 9C) and contralateral hippocampus (SO, CA1, SR, SL, and CA3; 9F). White arrows point to the LRRC8A signal that colocalizes with the NeuN signal. Scale bar: 50  $\mu$ m.

SL—and a notable increase in Gls1 immunoreactivity in  $GCL_U$  (all  $P < .05$  by  $t$ -test or Mann–Whitney–Wilcoxon test) (Figure 11B). As for the contralateral hippocampus, no change in total Gls1 immunoreactivity was detected (Mann–Whitney  $U = 19$ ,  $P = .0510$ , two-tailed  $t$ -test); however, layer-specific decreases were observed in SLM and SL (all  $P < .05$  by  $t$ -test or Mann–Whitney–Wilcoxon test) (Figure 11C).

Furthermore, in the ipsilateral hippocampus, total GS immunoreactivity was increased in KA-treated animals compared to controls at 7dKA (Mann–Whitney  $U = 7$ ,  $P = .0104$  two-tailed  $t$ -test) (Figure 12A), with layer-specific increases found in SO, CA1, and CA3—and a notable decrease in GS immunoreactivity in H (all  $P < .05$  by Mann–Whitney–Wilcoxon test) (Figure 12B). Similarly, in the contralateral hippocampus, total GS immunoreactivity was increased in KA-treated animals compared to controls (Mann–Whitney  $U = 16$ ,  $P = .0186$  two-tailed  $t$ -test), with increases observed in SO, CA1, and SR—and a notable decrease in GS immunoreactivity in  $GCL_U$  (all  $P < .05$  by Mann–Whitney–Wilcoxon test) (Figure 12C).

Taken together, at the early epileptogenic timepoint (7dKA) which coincides with the increased expression and immunolabeling of LRRC8A, there is marked downregulation of both GAD67 and glutaminase and an upregulation of GS in the total ipsilateral hippocampus. Contralaterally, GAD67 signal was decreased, no changes were observed in glutaminase, while GS signal was elevated. Figure 13 illustrates the divergent glutamate landscape of the ipsilateral (Figure 13A) and contralateral (Figure 13B) hippocampus at 7dKA, while Figure 14 summarizes the layer-specific dysregulation of glutamate-handling

machinery in the ipsilateral (Figure 14A) and contralateral (Figure 14B) hippocampus at 7dKA.

## Discussion

In this study, we used the IHKA model of MTLE to evaluate potential cell-type specific alterations in the pore-forming subunit of the VRAC, LRRC8A, during epileptogenesis. Using a Western blot protocol that was validated using SWELL1<sup>fl/fl</sup>; Nestin<sup>CRE/+</sup> mice as a negative control, we observed the upregulation of ipsilateral and contralateral dorsal hippocampal LRRC8A expression at 14dKA. Further analysis by IHC revealed increased immunolabeling for LRRC8A at 7dKA, which was colocalized and upregulated mainly in GFAP<sup>+</sup> cells. Further analysis of glutamate/GABA–glutamine cycle enzymes by IHC in the hippocampus at this early timepoint showed decreases in GAD67 and glutaminase, with increased labeling of GS. These findings suggest robust regulation of hippocampal LRRC8A during early epileptogenesis in conjunction with other components of the glutamate/GABA–glutamine cycle.

The injection of kainate into the murine hippocampus induces status epilepticus, followed by a latency period of no seizure activity and then the precipitation of spontaneous seizures—as observed in the human condition of MTLE (Riban et al., 2002). IHKA also produces inter-individual variation in ASD response, making it an attractive model for drug-resistant MTLE (Klein et al., 2015; Lévesque and Avoli, 2013). For this reason, we used the IHKA animal

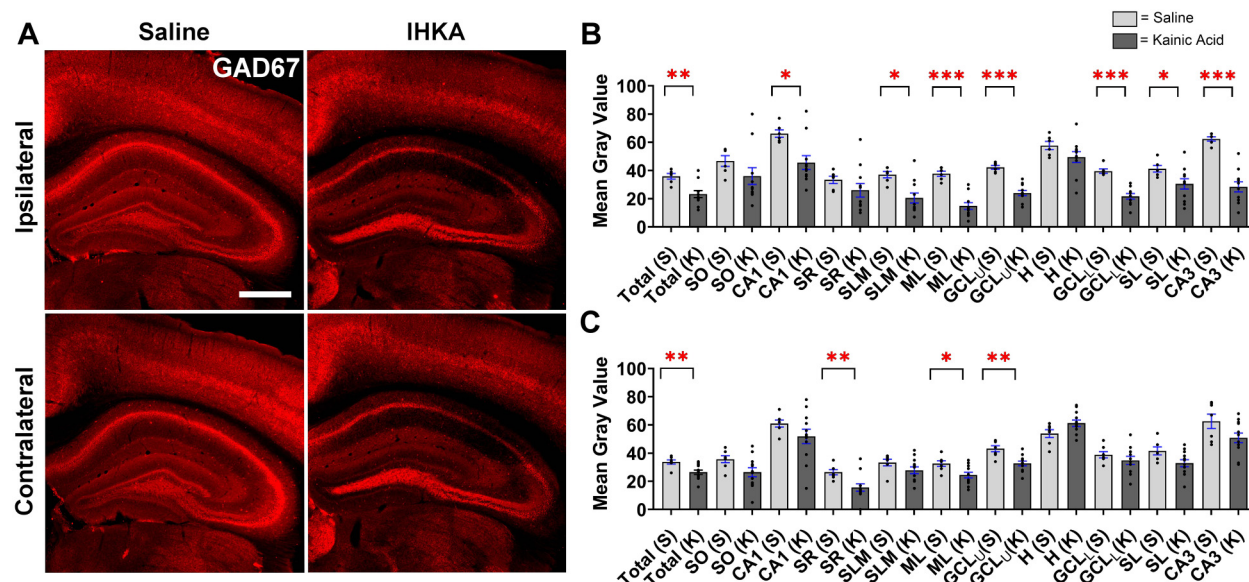


**Figure 10.** GAD67 immunoreactivity in the ipsilateral and contralateral dorsal hippocampus at 7dKA. (10A) Representative images of the dorsal hippocampus of saline-treated and KA-treated tissues at 7dKA stained for GAD67 (red). Total hippocampus and layer-specific quantification of GAD67 mean gray values in the ipsilateral (10B) and contralateral (10C) hippocampus ( $n = 6$  KA-treated animals and  $n = 5$  saline-treated animals, 1–2 sections/animal). \* indicates  $P < .05$ , \*\* indicates  $P < .01$ , and \*\*\* indicates  $P < .001$ . Scale bar: 500  $\mu\text{m}$ .



model of MTLE to study the regulation of LRRC8A—the essential subunit of VRAC—throughout MTLE.

VRACs are a group of ubiquitously expressed outwardly-rectifying channels that are composed of LRRC8 subunits, with LRRC8A being obligatory for pore formation (Ghouli et al., 2022; Qiu et al., 2014; Voss et al., 2014). In the presence of ATP, these channels are activated by cell swelling and mediate RVD through the efflux of various anions and osmolytes, including glutamate (Okada et al., 2021). The glutamate-releasing nature of VRAC has brought this family of channels to the attention of groups studying glutamate-mediated toxicity and ischemia. The deletion of LRRC8A from GFAP<sup>+</sup> astrocytes reduced glutamate-dependent neuronal excitability and protected against ischemia-mediated brain damage in an experimental model of stroke (Yang et al., 2019). Similarly, the deletion of LRRC8A from nestin<sup>+</sup> cells attenuated ischemia-induced glutamate release as determined through brain slice electrophysiology (Wilson et al., 2021). Given that epilepsy is a chronic seizure disorder characterized by neuronal hyperexcitability attributed to increased glutamatergic neurotransmission, it is critical to determine whether VRACs are also implicated in the genesis of seizures and epilepsy syndromes.

We were interested in answering three primary questions: (1) Is hippocampal LRRC8A dysregulated throughout the development and progression of MTLE?; (2) What are the time point of maximal dysregulation and the cell-type specificity of LRRC8A regulation?; and (3) Are there concurrent changes to other glutamate/GABA-glutamine cycle components at the timepoint of maximal LRRC8A dysregulation?

First, our data suggest that LRRC8A is indeed dysregulated throughout epileptogenesis. Immunoblot data derived from whole dorsal hippocampal tissue homogenate showed that LRRC8A is upregulated at 14dKA bilaterally, and IHC data derived from hippocampal tissue sections proximal to the injection site showed LRRC8A upregulation at 7dKA bilaterally. Layer-specific analysis revealed a more nuanced dysregulation of hippocampal LRRC8A at 1dKA, 7dKA, and 30dKA. The conflicting immunoblot and IHC findings may be rooted to the fact that biological tissues respond to focal insults with spatially dependent differential expression (Walls et al., 2023). In other words, LRRC8A expression from sections proximal to the injection site reflects more immediate cellular changes—explaining increases at 7dKA detected *via* IHC—whereas changes to the LRRC8A expression in the entire dorsal hippocampus develop over a longer period—explaining the delayed upregulation at 14dKA detected *via* immunoblot. The difference in the findings may also be a result of variable immunodetection, as two different anti-LRRC8A antibodies were used for each technique. In either case, we determined that LRRC8A is likely upregulated at the early- to mid-epileptogenic period, which corresponds to the period during which spontaneous seizures develop in our model.

Interestingly, both the immunoblot and IHC data point to the dysregulation of LRRC8A in the contralateral (uninjected) hippocampus. Unilateral kainate injection into the murine hippocampus has previously been shown to elicit seizures in bilateral hippocampi and cortices (Lisgaras and Scharfman, 2022). This finding points to the capacity of focal-onset

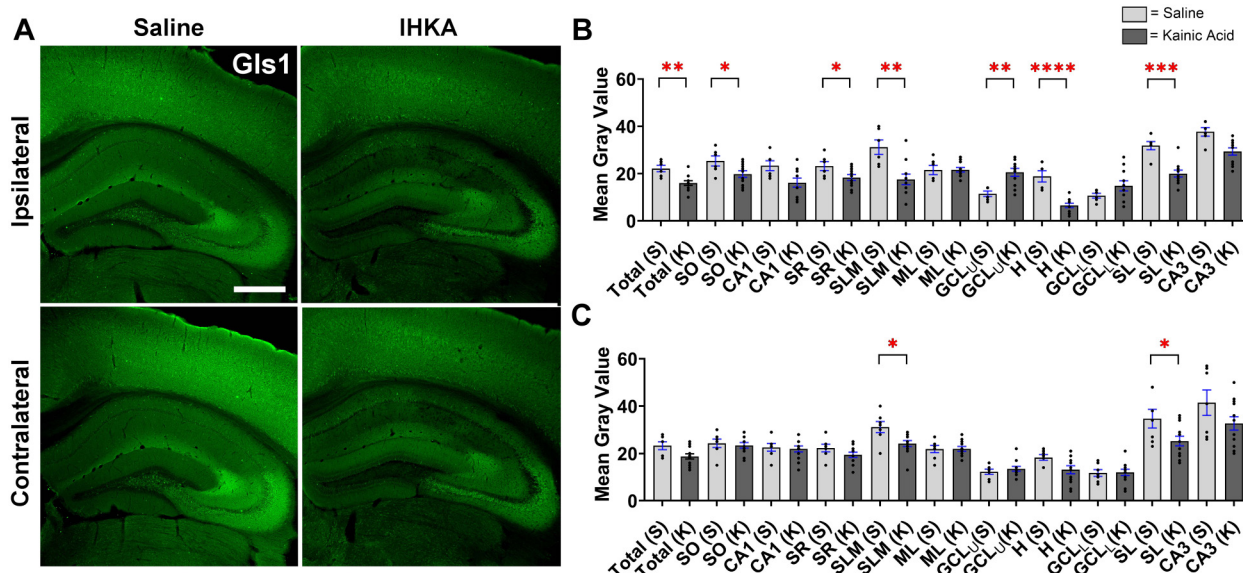


**Figure 11.** Glutaminase immunoreactivity in the ipsilateral and contralateral dorsal hippocampus at 7dKA. (11A) Representative images of the dorsal hippocampus of saline-treated and KA-treated tissues at 7dKA stained for glutaminase (Gls1, green). Total hippocampus and layer-specific quantification of Gls1 mean gray values in the ipsilateral (11B) and contralateral (11C) hippocampus ( $n = 6$  KA-treated animals and  $n = 5$  saline-treated animals, 1–2 sections/animal). \* indicates  $P < .05$ , \*\* indicates  $P < .01$ , \*\*\* indicates  $P < .001$ , and \*\*\*\* indicates  $P < .0001$ . Scale bar: 500  $\mu\text{m}$ .

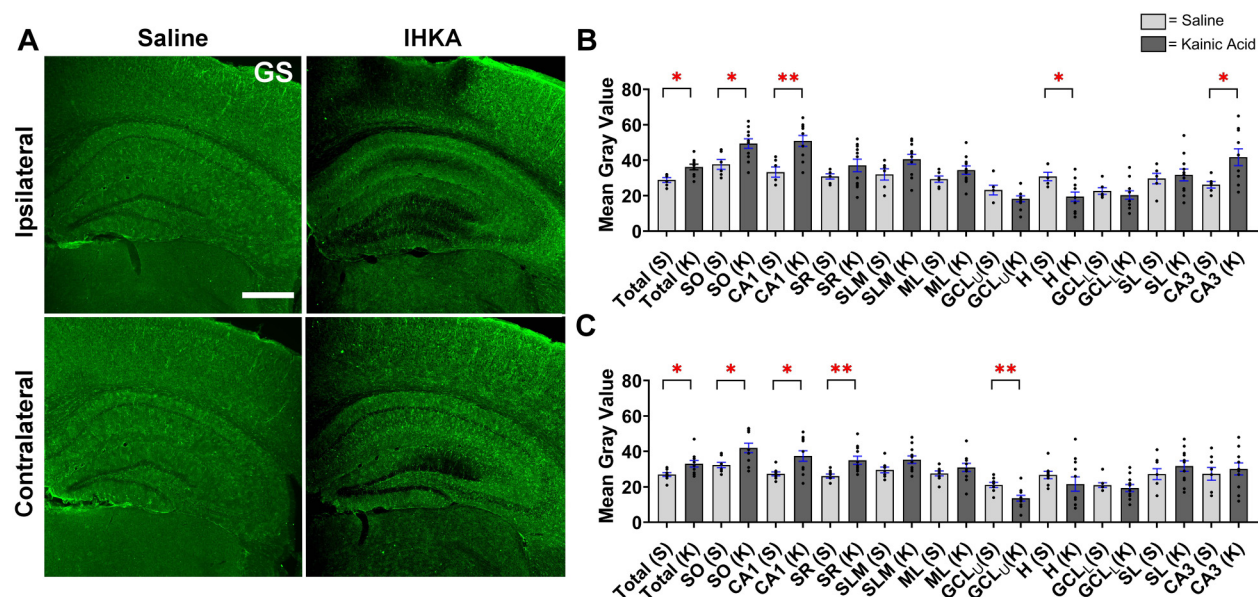


**Figure 12.** Glutamine synthetase immunoreactivity in the ipsilateral and contralateral dorsal hippocampus at 7dKA. (12A) Representative images of the dorsal hippocampus of saline-treated and KA-treated tissues at 7dKA stained for glutamine synthetase (GS, green). Total hippocampus and layer-specific quantification of GS mean gray values in the ipsilateral (12B) and contralateral (12C) hippocampus ( $n = 5$  KA-treated and saline-treated animals each, 1–2 sections/animal). \* indicates  $P < .05$  and \*\* indicates  $P < .01$ . Scale bar: 500  $\mu\text{m}$ .

seizures in MTLE to generalize and spread into the contralateral hemisphere of the brain. Based on this, the upregulation of LRRC8A observed in the contralateral hippocampus is likely a function of the propagated seizure activity, as opposed to a secondary response to the inflammation or neurotoxicity generated locally by the kainate injection.

Our finding that hippocampal LRRC8A is upregulated in epilepsy aligns with a previous study that showed increased hippocampal LRRC8A mRNA levels in epileptic tissue; however, we are weary to over-compare our results because they used a different method of KA administration (intraperitoneal vs. intrahippocampal), employed a different rodent model (rats vs. mice), and measured LRRC8A mRNA at a different timepoint (8-weeks vs. 1-, 7-, 14-, and 30-days) (Tsverava et al., 2019). Furthermore, we measured protein immunoreactivity whereas they measured mRNA levels, and it has been well established that the correlation between mRNA expression and protein expression is poor with a reported Pearson coefficient of 0.40 (Vogel and Marcotte, 2012). This suggests that only 40% of protein expression can be predicted by known mRNA measurements, and the remaining 60% variability is accounted for due to other regulatory mechanisms at the transcription level.

Regarding our second question, we aimed to determine the time point and cell-type specificity of maximal LRRC8A dysregulation. Using IHC, we found a remarkable increase in LRRC8A labeling at 7dKA bilaterally in the hippocampus. At this early epileptogenic period, colocalization of LRRC8A with GFAP suggests that LRRC8A upregulation occurs primarily in astrocytes bilaterally. Interestingly, the

ipsilateral epileptic hippocampus exhibits a higher gross labeling of astroglial LRRC8A compared to the contralateral epileptic hippocampus; however, the contralateral epileptic hippocampus exhibits a more robust increase in astroglial LRRC8A compared to contralateral nonepileptic controls. We detected minimal colocalization of LRRC8A in NeuN<sup>+</sup> neurons in the ipsilateral epileptic hippocampus compared to nonepileptic controls. However, there was no detectable trace of LRRC8A and NeuN colocalization in the contralateral epileptic hippocampus compared to nonepileptic controls. Importantly, although we detected “basal” astroglial LRRC8A colocalization in control tissues, we did not detect any neuronal LRRC8A expression in control tissues, suggesting an unappreciable expression of basal neuronal LRRC8A. Taken together, we found that in the control hippocampus, LRRC8A is expressed primarily by astrocytes bilaterally, and in the epileptic hippocampus, LRRC8A is upregulated primarily by astrocytes bilaterally.

As for our third question, we aimed to determine whether there are concurrent changes to other glutamate-GABA/glutamine cycle components at the timepoint of maximal LRRC8A dysregulation. It was previously determined that at this early epileptogenic period, the astrocytic glutamate transporter GLT-1 is downregulated in the dentate gyrus, the astrocytic glutamate transporter GLAST exhibits no dysregulation, and the neuronal glutamate transporter EAAC1 is downregulated in the ipsilateral hippocampal CA1 domain (Peterson and Binder, 2019; Peterson et al., 2021). These findings demonstrated significant disruption to glutamate reuptake mechanisms in the epileptic hippocampus. To

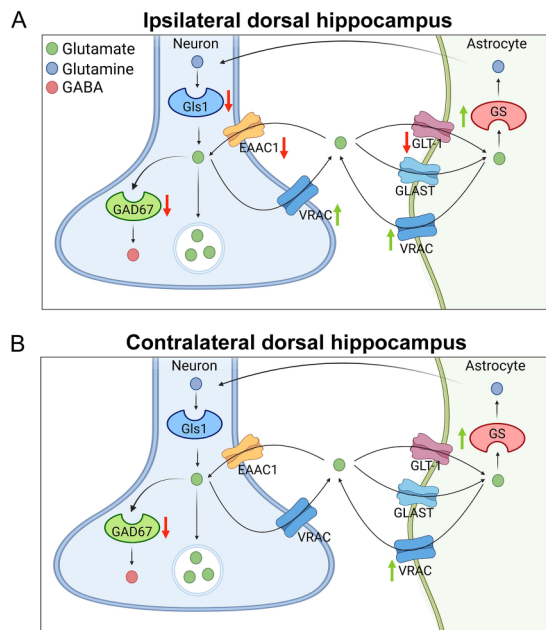


**Figure 13.** Diagrammatic summary of the regulation of key glutamate/GABA-glutamine proteins at 7dKA in the epileptic hippocampus. The figure illustrates key players in the glutamate/GABA-glutamine cycle between neurons and astrocytes, including VRAC (LRRC8A), astrocytic glutamate transporters GLT-1 and GLAST, neuronal glutamate transporter EAAC1, astrocytic enzyme GS, neuronal enzymes Gls1 and GAD67, as well as the neurotransmitters glutamate, glutamine, and GABA. Upward green arrows represent upregulation and downward red arrows represent downregulation of the transporters, channels, and enzymes at 7dKA in the ipsilateral (13A) and contralateral (13B) hippocampus. Partly created with BioRender.com.

build on these findings and to develop a more comprehensive picture of the glutamate landscape at 7dKA, we aimed to determine whether GAD67, Gls1, and GS were dysregulated at this early epileptogenic timepoint.

GAD is an enzyme primarily expressed in inhibitory neurons that catalyzes the conversion of glutamate into GABA, the inhibitory neurotransmitter responsible for the modulation of neuronal network excitability (Neuray et al., 2020). GAD exists in two isoforms: GAD65 and GAD67, with the latter contributing to greater than 90% of basal GABA in the brain (Neuray et al., 2020). The inhibition of GAD67 has previously been shown to induce drug-resistant epilepsy in a zebrafish model, and mice deficient in GAD65 develop spontaneous seizures (Dudek and Shao, 2003; Zhang et al., 2017). Furthermore, bi-allelic *GAD1* gene variants were observed in humans with early-infantile onset epilepsy (Neuray et al., 2020). These data point to the critical role of this enzyme in modulating neuronal excitability, and they suggest that GAD dysregulation can lead to aberrant neuronal activity. Similarly, our data suggest that GAD67 was significantly downregulated in both the ipsilateral and

contralateral epileptic hippocampus. This would effectively decrease the conversion of glutamate to GABA, leading to glutamate accumulation in the inhibitory cells of the hippocampus. Humans and animal models of MTLLE exhibit a loss of inhibitory neurons—particularly in the hippocampal dentate gyrus—that precedes the onset of seizure activity (Dudek and Shao, 2003). Based on this, the downregulation of GAD67 and the subsequent accumulation of glutamate in inhibitory neurons may precipitate the death of this subset of neurons, as is characteristic of the epileptic tissue. A recent study found that the overexpression of inhibitory parvalbumin interneurons correlates with an upregulation of GAD65 and GAD67, which in turn results in increased GABA levels and decreased glutamate levels (Zeng et al., 2023). Reciprocally, they found that the silencing of parvalbumin cells downregulates GAD65 and GAD67, leading to decreased GABA levels and increased glutamate levels (Zeng et al., 2023). Taken together, these novel findings suggest that restoration or the upregulation of GAD67 may be neuroprotective and/or antiepileptogenic in this model.

Glutaminase is a mitochondrial enzyme that catabolizes glutamine (an “inert” neurotransmitter) into glutamate and ammonia. This enzyme exists in two isoforms: kidney-type Gls1, which is expressed robustly in the brain, and liver-type Gls2 (Curthoys and Watford, 1995). Gls1 is primarily expressed in neuronal mitochondria; however, minimal protein expression was also identified in astrocytes (Cardona et al., 2015). Loss of function mutations to the *Gls* gene in humans have been shown to cause lethal early neonatal encephalopathy (Rumping et al., 2019). Encephalopathies and seizures are often entangled—albeit mechanistically elusive—phenomena (LaRoche, 2011). Therefore, it is possible that *Gls* deficiencies that manifest as neonatal encephalopathies share underlying undetected seizure pathologies. Previous studies have shown that *Gls* mRNA is increased in the dentate gyrus of patients with MTLLE compared to nonepilepsy controls (Eid et al., 2013). In our study, however, we determined that Gls1 (isoforms KCA and GAC) was downregulated in the ipsilateral epileptic hippocampus. Although this may appear to contradict previous reports, it is important to note that the correlation between mRNA levels and protein levels is often weak, and discrepancies can be attributed to the various phases of regulation that occur between transcription and translation (Koussounadis et al., 2015). Dissimilar findings in the literature may also be a function of the different models and time points that are studied. Our observation that Gls1 is decreased may suggest that less glutamine is being converted to glutamate in the ipsilateral epileptic hippocampus, which would appear to be a favorable compensation as it implies that there is a reduction in glutamate levels. However, additional studies would be necessary to quantify the glutamate content of the epileptic tissue. Antithetical to any benefits derived from decreased glutamate levels, the accumulation of intracellular glutamine is hypothesized to exert its own



**A Ipsilateral dorsal hippocampus**

Biomarker	SO	CA1	SR	SLM	ML	GCL <sub>U</sub>	H	GCL <sub>L</sub>	SL	CA3
LRRRC8A		↑				↑			↑	↑
GAD67		↓		↓	↓	↓		↓	↓	↓
Gls1	↓		↓	↓		↑	↓		↓	
GS	↑	↑					↓			↑
GLAST (EAAT1)										
GLT-1 (EAAT2)						↓		↓		
EAAC1 (EAAT3)	↓	↓	↓	↓						

**B Contralateral dorsal hippocampus**

Biomarker	SO	CA1	SR	SLM	ML	GCL <sub>U</sub>	H	GCL <sub>L</sub>	SL	CA3
LRRRC8A	↑	↑	↑						↑	↑
GAD67			↓		↓	↓				
Gls1				↓					↓	
GS	↑	↑	↑			↓				
GLAST (EAAT1)										
GLT-1 (EAAT2)										
EAAC1 (EAAT3)										

**Figure 14.** Graphical summary of layer-specific regulation of key glutamate/GABA-glutamine proteins at 7dKA in the epileptic hippocampus. The graph summarizes the layer specific changes to the levels of LRRRC8A, GAD67, Gls1, GS, GLAST (EAAT1), GLT-1 (EAAT2), and EAAC1 (EAAT3) in the epileptogenic ipsilateral (14A) and contralateral (14B) dorsal hippocampus. Green upward arrows represent upregulation, red downward arrows represent downregulation, and empty boxes represent no changes in the biomarker expression. Partly created with BioRender.com.

toxicity, as it excessively transports ammonia into the mitochondria, interfering with normal mitochondrial function (Albrecht and Norenberg, 2006). Given that epileptic seizures often result from mitochondrial dysfunction, the downregulation of glutaminase and the subsequent increase in glutamine concentration may serve as a mechanism by which mitochondrial pathology manifests (Fabisiak and Patel, 2022; Fulton et al., 2021; Gano et al., 2018; Patel, 2004).

GS is an enzyme that is primarily expressed in the astroglial cytoplasm (particularly at perivascular endfeet) and works to metabolize glutamate and ammonia into glutamine (Eid et al., 2012). GS downregulation is implicated in many neurological diseases such as Alzheimer's, depression, and schizophrenia (Eid et al., 2012). Previous studies have shown that GS is downregulated in resected hippocampal tissues from MTL patients, suggesting that decreased GS expression and the subsequent accumulation of glutamate

leads to neuronal hypersynchrony and seizures (Eid et al., 2004). In fact, from the case study of a 3-year-old patient, we found that genetic GS deficiency led to the development of neonatal seizures and encephalopathy (Häberle et al., 2011). Despite these findings, we observed increased GS immunolabeling in both the ipsilateral and contralateral epileptic hippocampus. Although these findings appear to be contradictory, it is important to note that we measured hippocampal GS at the early epileptogenic phase (7dKA) of MTL. We hypothesize that the acute phase of temporal lobe epileptogenesis is characterized by a compensatory upregulation of GS, with astrocytes working in overdrive to decrease the glutamate levels. However, at later timepoints coinciding with prolonged neuroinflammation when the hippocampus undergoes sclerosis and the glia become chronically hypertrophic, a pathological downregulation of astroglial GS ensues.

In summary, our findings suggest that LRRC8A—and therefore VRAC—are upregulated primarily in GFAP<sup>+</sup> astrocytes as early as 7dKA, coinciding with the timepoint of spontaneous seizure onset in this model. Concurrently, GAD67, Gsl1, and GS are also dysregulated at this timepoint. Because most studies point to the excitotoxic effects of VRAC-mediated glutamate release, we speculate that the increase in astroglial VRAC protein expression is proportional to the increase in channel activity, resulting in increased VRAC-mediated glutamate efflux into the extracellular space. In fact, the dysregulation of VRAC may work in concert with the dysregulation of the other glutamate-GABA/glutamine cycle players to push the hippocampus towards a hypersynchronous state and precipitate the onset of spontaneous seizures. Specifically, glutamate transporter downregulation, LRRC8A upregulation, and GAD67 downregulation may increase extracellular glutamate levels. The net effect of these aberrant transporters, channels, and enzymes could be excitotoxic damage to the brain tissue and the precipitation of seizures.

Alternately, it is possible that an increased channel expression may not directly correlate with increased channel activity. One study found that the overexpression of *lrrc8aa* (the zebrafish equivalent of LRRC8A) in HPF cells reduced swell-activated chloride currents, suggesting the increase of the essential pore-forming subunit does not increase the VRAC function (Yamada et al., 2016). However, it is important to consider that the physiological consequences of exogenous overexpression may differ from that of endogenous upregulation. The exogenous overexpression of LRRC8A may cause the formation of LRRC8A homomeric VRAC channels that poorly recapitulate normal VRAC activity, whereas the endogenous upregulation of LRRC8A may parallel the upregulation of other LRRC8 subunits that together assemble into functional VRAC channels (Yamada et al., 2021).

It is also important to note that recent studies have challenged the primary narrative of VRAC-mediated glutamatergic excitotoxicity. One group found that the total deletion of LRRC8A in nestin<sup>+</sup> cells resulted in complete loss of VRAC-mediated glutamate release, whereas heterozygous knockout animals exhibited full swell-activated glutamate release (Balkaya et al., 2023). Despite this difference, both full and heterozygous knockout animals displayed identical protection against ischemia in an experimental stroke model, suggesting VRAC ablation may exert its neuroprotective function through nonglutamatergic mechanisms (Balkaya et al., 2023).

Although it is clear that LRRC8A—and, by extension, VRAC—are upregulated in the epileptic hippocampus, the functional effects of the upregulation remain unclear. Further studies are required to delineate the role of VRAC in excitotoxicity and epileptogenesis. To evaluate whether cell-type specific VRAC play a causative role in the development, progression, and termination of spontaneous seizures, video-EEG studies should be conducted in conjunction with the use of either VRAC inhibitors or transgenic LRRC8A knockout/ knockdown animals in appropriate animal models of epileptogenesis.

## Abbreviations

MTLE	mesial temporal lobe epilepsy
ASDs	anti-seizure drugs
GLT-1	glutamate transporter 1
GLAST	glutamate-aspartate transporter
EAAC1	excitatory amino acid transporter 1
VRAC	volume regulated anion channel
LRRC8A	leucine-rich repeating protein 8A
IHKA	intrahippocampal kainic acid
KA	kainic acid
1dKA	1-day post-IHKA
7dKA	7-days post-IHKA
14dKA	14-days post-IHKA
30dKA	30-days post-IHKA
HS	hippocampal sclerosis
SE	status epilepticus
GCL	granule cell layer
SO	stratum oriens
SR	status radiatum
SLM	stratum lacunosum moleculare
ML	molecular layer
SL	stratum lucidum
GFAP	glial fibrillary acidic protein
GAD67	glutamic acid decarboxylase isoform 67
Gsl1	glutaminase type 1
GS	glutamate synthetase
GABA	gamma aminobutyric acid.

## Acknowledgements

We thank Pedro Villa from the Lab of Djurdjica Coss at the UCR for sharing Fiji Image-J software compatible colocalization plug-in.

## Author Contributions

MRG made substantial contributions to the design of the work, acquisition, analysis, interpretation of the data, and drafting of the article. CRJ made substantial contributions to the concept, design, and optimization of techniques used. RS and TAF contributed to the design of the work. DKB and TAF made substantial contributions to the design and oversight of the work and revised the article critically. All authors approved the final version of the manuscript.


## Declaration of Conflicting Interests

The author(s) declare no potential conflicts of interest with respect to the research, authorship, and/or publication of this article.

## Funding

The author(s) received no financial support for the research, authorship, and/or publication of this article.

## ORCID iD

Devin K. Binder  <https://orcid.org/0000-0003-1597-5604>

## References

- Albrecht, J., & Norenberg, M. D. (2006). Glutamine: A Trojan horse in ammonia neurotoxicity. *Hepatology*, *44*(4), 788–794. <https://doi.org/10.1002/hep.21357>
- Balkaya, M., Dohare, P., Chen, S., Schober, A. L., Fidaleo, A. M., Nalwalk, J. W., Sah, R., & Mongin, A. A. (2023). Conditional deletion of LRRC8A in the brain reduces stroke damage independently of swelling-activated glutamate release. *iScience*, *26*(5), 106669. <https://doi.org/10.1016/j.isci.2023.106669>
- Baulac, M. (2015). MTLE With hippocampal sclerosis in adult as a syndrome. *Revue Neurologique (Paris)*, *171*(3), 259–266. <https://doi.org/10.1016/j.neurol.2015.02.004>
- Beghi, E. (2020). The epidemiology of epilepsy. *Neuroepidemiology*, *54*(2), 185–191. <https://doi.org/10.1159/000503831>
- Bernal, A., & Arranz, L. (2018). Nestin-expressing progenitor cells: Function, identity and therapeutic implications. *Cellular and Molecular Life Sciences*, *75*(12), 2177–2195. <https://doi.org/10.1007/s00018-018-2794-z>
- Bukke, V. N., Archana, M., Villani, R., Romano, A. D., Wawrzyniak, A., Balawender, K., Orkisz, S., Beggiato, S., Serviddio, G., & Cassano, T. (2020). The dual role of glutamatergic neurotransmission in Alzheimer's disease: From pathophysiology to pharmacotherapy. *International Journal of Molecular Sciences*, *21*(20), 7452. <https://doi.org/10.3390/ijms21207452>
- Cardona, C., Sánchez-Mejías, E., Dávila, J. C., Martín-Rufián, M., Campos-Sandoval, J. A., Vitorica, J., Alonso, F. J., Matés, J. M., Segura, J. A., Norenberg, M. D., Rama Rao, K. V., Jayakumar, A. R., Gutiérrez, A., & Márquez, J. (2015). Expression of Gls and Gls2 glutaminase isoforms in astrocytes. *Glia*, *63*(3), 365–382. <https://doi.org/10.1002/glia.22758>
- Curthoys, N. P., & Watford, M. (1995). Regulation of glutaminase activity and glutamine metabolism. *Annual Review of Nutrition*, *15*, 133–159. <https://doi.org/10.1146/annurev.nu.15.070195.001025>
- Dudek, F. E., & Shao, L. R. (2003). Loss of GABAergic interneurons in seizure-induced epileptogenesis. *Epilepsy Currents / American Epilepsy Society*, *3*(5), 159–161. <https://doi.org/10.1046/j.1535-7597.2003.03503.x>
- Eid, T., Behar, K., Dhaher, R., Bumanglag, A. V., & Lee, T. S. (2012). Roles of glutamine synthetase inhibition in epilepsy. *Neurochemical Research*, *37*(11), 2339–2350. <https://doi.org/10.1007/s11064-012-0766-5>
- Eid, T., Lee, T. S., Wang, Y., Perez, E., Drummond, J., Lauritzen, F., Bergersen, L. H., Meador-Woodruff, J. H., Spencer, D. D., de Lanerolle, N. C., & McCullumsmith, R. E. (2013). Gene expression of glutamate metabolizing enzymes in the hippocampal formation in human temporal lobe epilepsy. *Epilepsia*, *54*(2), 228–238. <https://doi.org/10.1111/epi.12008>
- Eid, T., Thomas, M. J., Spencer, D. D., Rundén-Pran, E., Lai, J. C., Malthankar, G. V., Kim, J. H., Danbolt, N. C., Ottersen, O. P., & de Lanerolle, N. C. (2004). Loss of glutamine synthetase in the human epileptogenic hippocampus: Possible mechanism for raised extracellular glutamate in mesial temporal lobe epilepsy. *Lancet*, *363*(9402), 28–37. [https://doi.org/10.1016/S0140-6736\(03\)15166-5](https://doi.org/10.1016/S0140-6736(03)15166-5)
- Engel, J. Jr. (2001). Mesial temporal lobe epilepsy: What have we learned? *Neuroscientist*, *7*(4), 340–352. <https://doi.org/10.1177/107385840100700410>
- Engel, J. Jr., M. P. McDermott, S. Wiebe, J. T. Langfitt, J. M. Stern, S. Dewar, M. R. Sperling, I. Gardiner, G. Erba, I. Fried, M. Jacobs, H. V. Vinters, S. Mintzer, & K. Kieburz (2012). Early surgical therapy for drug-resistant temporal lobe epilepsy: A randomized trial. *Journal of the American Medical Association*, *307*(9), 922–930. <https://doi.org/10.1001/jama.2012.220>
- Fabisiak, T., & Patel, M. (2022). Crosstalk between neuroinflammation and oxidative stress in epilepsy. *Frontiers in Cell and Developmental Biology*, *10*, 976953. <https://doi.org/10.3389/fcell.2022.976953>
- Formaggio, F., Saracino, E., Mola, M. G., Rao, S. B., Amiry-Moghaddam, M., Muccini, M., Zamboni, R., Nicchia, G. P., Caprini, M., & Benfenati, V. (2019). LRRC8A Is essential for swelling-activated chloride current and for regulatory volume decrease in astrocytes. *FASEB Journal*, *33*(1), 101–113. <https://doi.org/10.1096/fj.201701397RR>
- Fulton, R. E., Pearson-Smith, J. N., Huynh, C. Q., Fabisiak, T., Liang, L. P., Aivazidis, S., High, B. A., Buscaglia, G., Corrigan, T., Valdez, R., Shimizu, T., & Patel, M. N. (2021). Neuron-specific mitochondrial oxidative stress results in epilepsy, glucose dysregulation and a striking astrocyte response. *Neurobiology of Disease*, *158*, 105470. <https://doi.org/10.1016/j.nbd.2021.105470>
- Gano, L. B., Liang, L. P., Ryan, K., Michel, C. R., Gomez, J., Vassilopoulos, A., Reisdorph, N., Fritz, K. S., & Patel, M. (2018). Altered mitochondrial acetylation profiles in a kainic acid model of temporal lobe epilepsy. *Free Radical Biology & Medicine*, *123*, 116–124. <https://doi.org/10.1016/j.freeradbiomed.2018.05.063>
- Ghouli, M. R., Fiacco, T. A., & Binder, D. K. (2022). Structure-function relationships of the LRRC8 subunits and subdomains of the volume-regulated anion channel (VRAC). *Frontiers in Cellular Neuroscience*, *16*, 962714. <https://doi.org/10.3389/fncel.2022.962714>
- Häberle, J., Shahbeck, N., Ibrahim, K., Hoffmann, G. F., & Ben-Omran, T. (2011). Natural course of glutamine synthetase deficiency in a 3 year old patient. *Molecular Genetics and Metabolism*, *103*(1), 89–91. <https://doi.org/10.1016/j.ymgme.2011.02.001>
- Hubbard, J. A., Szu, J. I., Yonan, J. M., & Binder, D. K. (2016). Regulation of astrocyte glutamate transporter-1 (GLT1) and aquaporin-4 (AQP4) expression in a model of epilepsy. *Experimental Neurology*, *283*(Pt A), 85–96. <https://doi.org/10.1016/j.expneurol.2016.05.003>
- Hyzinski-García, M. C., Rudkouskaya, A., & Mongin, A. A. (2014). LRRC8A Protein is indispensable for swelling-activated and ATP-induced release of excitatory amino acids in rat astrocytes. *Journal of Physiology*, *592*(22), 4855–4862. <https://doi.org/10.1113/jphysiol.2014.278887>
- Klein, S., Bankstahl, M., & Löscher, W. (2015). Inter-individual variation in the effect of antiepileptic drugs in the intrahippocampal kainate model of mesial temporal lobe epilepsy in mice. *Neuropharmacology*, *90*, 53–62. <https://doi.org/10.1016/j.neuropharm.2014.11.008>
- Koussounadis, A., Langdon, S. P., Um, I. H., Harrison, D. J., & Smith, V. A. (2015). Relationship between differentially expressed mRNA and mRNA-protein correlations in a xenograft model system. *Scientific Reports*, *5*(1), 10775. <https://doi.org/10.1038/srep10775>
- Kwan, P., & Brodie, M. J. (2000). Early identification of refractory epilepsy. *New England Journal of Medicine*, *342*(5), 314–319. <https://doi.org/10.1056/NEJM200002033420503>
- LaRoche, S. M. (2011). Seizures and encephalopathy. *Seminars in Neurology*, *31*(2), 194–201. <https://doi.org/10.1055/s-0031-1277987>

- Lee, D. J., Hsu, M. S., Seldin, M. M., Arellano, J. L., & Binder, D. K. (2012). Decreased expression of the glial water channel aquaporin-4 in the intrahippocampal kainic acid model of epileptogenesis. *Experimental Neurology*, *235*(1), 246–255. <https://doi.org/10.1016/j.expneurol.2012.02.002>
- Lévesque, M., & Avoli, M. (2013). The kainic acid model of temporal lobe epilepsy. *Neuroscience & Biobehavioral Reviews*, *37*(10), 2887–2899. <https://doi.org/10.1016/j.neubiorev.2013.10.011>
- Lisgaras, C. P., & Scharfman, H. E. (2022). Robust chronic convulsive seizures, high frequency oscillations, and human seizure onset patterns in an intrahippocampal kainic acid model in mice. *Neurobiology of Disease*, *166*, 105637. <https://doi.org/10.1016/j.nbd.2022.105637>
- Neuray, C., et al. (2020). Early-infantile onset epilepsy and developmental delay caused by bi-allelic GAD1 variants. *Brain*, *143*(8), 2388–2397. <https://doi.org/10.1093/brain/awaa178>
- Okada, Y., Sabirov, R. Z., Sato-Numata, K., & Numata, T. (2021). Cell death induction and protection by activation of ubiquitously expressed anion/cation channels. Part 1: Roles of VSOR/VRAC in cell volume regulation, Release of double-edged signals and apoptotic/necrotic cell death. *Frontiers in Cell and Developmental Biology*, *8*, 1–12. <https://doi.org/10.3389/fcell.2020.614040>
- Patel, M. (2004). Mitochondrial dysfunction and oxidative stress: Cause and consequence of epileptic seizures. *Free Radical Biology & Medicine*, *37*(12), 1951–1962. <https://doi.org/10.1016/j.freeradbiomed.2004.08.021>
- Peterson, A. R., & Binder, D. K. (2019). Regulation of synaptosomal GLT-1 and GLAST during epileptogenesis. *Neuroscience*, *411*, 185–201. <https://doi.org/10.1016/j.neuroscience.2019.05.048>
- Peterson, A. R., Garcia, T. A., Ford, B. D., & Binder, D. K. (2021). Regulation of NRG-1-ErbB4 signaling and neuroprotection by exogenous neuregulin-1 in a mouse model of epilepsy. *Neurobiology of Disease*, *161*, 105545. <https://doi.org/10.1016/j.nbd.2021.105545>
- Qiu, Z., Dubin, A. E., Mathur, J., Tu, B., Reddy, K., Miraglia, L. J., Reinhardt, J., Orth, A. P., & Patapoutian, A. (2014). SWELL1, A plasma membrane protein, is an essential component of volume-regulated anion channel. *Cell*, *157*(2), 447–458. <https://doi.org/10.1016/j.cell.2014.03.024>
- Racine, R. J. (1972). Modification of seizure activity by electrical stimulation: II. Motor seizure. *Electroencephalography and Clinical Neurophysiology*, *32*(3), 281–294. [https://doi.org/10.1016/0013-4694\(72\)90177-0](https://doi.org/10.1016/0013-4694(72)90177-0)
- Riban, V., Bouillere, V., Pham-Lê, B. T., Fritschy, J. M., Marescaux, C., & Depaulis, A. (2002). Evolution of hippocampal epileptic activity during the development of hippocampal sclerosis in a mouse model of temporal lobe epilepsy. *Neuroscience*, *112*(1), 101–111. [https://doi.org/10.1016/S0306-4522\(02\)00064-7](https://doi.org/10.1016/S0306-4522(02)00064-7)
- Rothstein, J. D., Dykes-Hoberg, M., Pardo, C. A., Bristol, L. A., Jin, L., Kuncl, R. W., Kanai, Y., Hediger, M. A., Wang, Y., Schielke, J. P., & Welty, D. F. (1996). Knockout of glutamate transporters reveals a major role for astroglial transport in excitotoxicity and clearance of glutamate. *Neuron*, *16*(3), 675–686. [https://doi.org/10.1016/S0896-6273\(00\)80086-0](https://doi.org/10.1016/S0896-6273(00)80086-0)
- Rumping, L., Büttner, B., Maier, O., Rehmann, H., Lequin, M., Schlump, J. U., Schmitt, B., Schieberger-Bronkhorst, B., Prinsen, H., Losa, M., Fingerhut, R., Lemke, J. R., Zwartkuis, F. J. T., Houwen, R. H. J., Jans, J. J. M., Verhoeven-Duif, N. M., van Hasselt, P. M., & Jamra, R. (2019). Identification of a loss-of-function mutation in the context of glutaminase deficiency and neonatal epileptic encephalopathy. *JAMA Neurology*, *76*(3), 342–350. <https://doi.org/10.1001/jamaneurol.2018.2941>
- Serra, S. A., Stojakovic, P., Amat, R., Rubio-Moscardo, F., Latorre, P., Seisenbacher, G., Canadell, D., Böttcher, R., Aregger, M., Moffat, J., de Nadal, E., Valverde, M. A., & Posas, F. (2021). LRRC8A-containing Chloride channel is crucial for cell volume recovery and survival under hypertonic conditions. *Proceedings of the National Academy of Sciences*, *118*(23), e2025013118. <https://doi.org/10.1073/pnas.2025013118>
- Tanaka, K., Watase, K., Manabe, T., Yamada, K., Watanabe, M., Takahashi, K., Iwama, H., Nishikawa, T., Ichihara, N., Kikuchi, T., Okuyama, S., Kawashima, N., Hori, S., Takimoto, M., & Wada, K. (1997). Epilepsy and exacerbation of brain injury in mice lacking the glutamate transporter GLT-1. *Science*, *276*(5319), 1699–1702. <https://doi.org/10.1126/science.276.5319.1699>
- Trinka, E., Cock, H., Hesdorffer, D., Rossetti, A. O., Scheffer, I. E., Shinnar, S., Shorvon, S., & Lowenstein, D. H. (2015). A definition and classification of status epilepticus – report of the ILAE task force on classification of Status epilepticus. *Epilepsia*, *56*(10), 1515–1523. <https://doi.org/10.1111/epi.13121>
- Tsverava, L., Kandashvili, M., Margvelani, G., Lortkipanidze, T., Gamkrelidze, G., Lepsveridze, E., Kokaia, M., & Solomonias, R. (2019). Long-Term effects of myoinositol on behavioural seizures and biochemical changes evoked by kainic acid induced epileptogenesis. *Biomed Research International*, *2019*, 4518160. <https://doi.org/10.1155/2019/4518160>
- Vogel, C., & Marcotte, E. M. (2012). Insights into the regulation of protein abundance from proteomic and transcriptomic analyses. *Nature Reviews Genetics*, *13*(4), 227–232. <https://doi.org/10.1038/nrg3185>
- Voss, F. K., Ullrich, F., Münch, J., Lazarow, K., Lutter, D., Mah, N., Andrade-Navarro, M. A., von Kries, J. P., Stauber, T., & Jentsch, T. J. (2014). Identification of LRRC8 heteromers as an essential component of the volume-regulated anion channel VRAC. *Science*, *344*(6184), 634–638. <https://doi.org/10.1126/science.1252826>
- Walls, G. M., Ghita, M., Queen, R., Edgar, K. S., Gill, E. K., Kuburas, R., Grievae, D. J., Watson, C. J., McWilliam, A., Van Herk, M., Williams, K. J., Cole, A. J., Jain, S., & Butterworth, K. T. (2023). Spatial gene expression changes in the mouse heart after base-targeted irradiation. *International Journal of Radiation Oncology Biology Physics*, *115*(2), 453–463. <https://doi.org/10.1016/j.ijrobp.2022.08.031>
- Wilson, C. S., Dohare, P., Orbeta, S., Nalwalk, J. W., Huang, Y., Ferland, R. J., Sah, R., Scimemi, A., & Mongin, A. A. (2021). Late adolescence mortality in mice with brain-specific deletion of the volume-regulated anion channel subunit LRRC8A. *FASEB Journal*, *35*(10), e21869. <https://doi.org/10.1096/fj.202002745R>
- Yamada, T., Figueroa, E. E., Denton, J. S., & Strange, K. (2021). LRRC8A Homohexameric channels poorly recapitulate VRAC regulation and pharmacology. *American Journal of Physiology-Cell Physiology*, *320*(3), C293–C303. <https://doi.org/10.1152/ajpcell.00454.2020>
- Yamada, T., Wondergem, R., Morrison, R., Yin, V. P., & Strange, K. (2016). Leucine-rich repeat containing protein LRRC8A is essential for swelling-activated Cl<sup>-</sup> currents and embryonic development in zebrafish. *Physiological Reports*, *4*(19), 1–11. <https://doi.org/10.14814/phy2.12940>
- Yang, J., Vitery, M. D. C., Chen, J., Osei-Owusu, J., Chu, J., & Qiu, Z. (2019). Glutamate-Releasing SWELL1 channel in astrocytes

- modulates synaptic transmission and promotes brain damage in stroke. *Neuron*, 102(4), 813–827.e816. <https://doi.org/10.1016/j.neuron.2019.03.029>
- Zeng, C., Lei, D., Lu, Y., Huang, Q., Wu, Y., Yang, S., & Wu, Y. (2023). Parvalbumin in the metabolic pathway of glutamate and  $\gamma$ -aminobutyric acid: Influence on expression of GAD65 and GAD67. *Archives of Biochemistry and Biophysics*, 734, 109499. <https://doi.org/10.1016/j.abb.2022.109499>
- Zhang, Y., Vanmeert, M., Siekierska, A., Ny, A., John, J., Callewaert, G., Lescrinier, E., Dehaen, W., de Witte, P. A. M., & Kaminski, R. M. (2017). Inhibition of glutamate decarboxylase (GAD) by ethyl ketopentenoate (EKP) induces treatment-resistant epileptic seizures in zebrafish. *Scientific Reports*, 7(1), 7195. <https://doi.org/10.1038/s41598-017-06294-w>
- Zhou, J. J., Luo, Y., Chen, S. R., Shao, J. Y., Sah, R., & Pan, H. L. (2020). LRRC8A-dependent volume-regulated anion channels contribute to ischemia-induced brain injury and glutamatergic input to hippocampal neurons. *Experimental Neurology*, 332, 113391. <https://doi.org/10.1016/j.expneurol.2020.113391>